IEEE Access
Multidisciplinary ⋮ Rapid Review ⋮ Open Access Journal

Received 18 July 2022, accepted 26 August 2022, date of publication 12 September 2022, date of current version 20 September 2022.

Digital Object Identifier 10.1109/ACCESS.2022.3205632

RESEARCH ARTICLE

Convergence Enhancement of Super-Twisting Sliding Mode Control Using Artificial Neural Network for DFIG-Based Wind Energy Conversion Systems

IRFAN SAMI[1], (Graduate Student Member, IEEE), SHAFAAT ULLAH[2,3], SAREER UL AMIN[4], AHMED AL-DURRA[5], (Senior Member, IEEE), NASIM ULLAH[6], AND JONG-SUK RO[1]

[1]School of Electrical and Electronics Engineering, Chung-Ang University, Dongjak-gu, Seoul 06974, South Korea
[2]Department of Electrical Engineering, University of Engineering and Technology Peshawar, Bannu Campus, Bannu 28100, Pakistan
[3]Department of Electrical and Computer Engineering, COMSATS University Islamabad, Abbottabad Campus, Abbottabad 22060, Pakistan
[4]Department of Computer Science and Engineering, Chung-Ang University, Dongjak-gu, Seoul 06974, South Korea
[5]Advanced Power and Energy Center, Electrical Engineering and Computer Science Department, Khalifa University, Abu Dhabi, United Arab Emirates
[6]Department of Electrical Engineering, College of Engineering, Taif University, Taif 21944, Saudi Arabia

Corresponding author: Jong-Suk Ro (jongsukro@gmail.com)

This work was supported in part by the Chung-Ang University Young Scientist Scholarship in 2022, and in part by the National Research Foundation of Korea (NRF) Grant through the Ministry of Science and ICT under Grant NRF-2022R1A2C2004874.

ABSTRACT The smooth and robust injection of wind power into the utility grid requires stable, robust, and simple control strategies. The super-twisting sliding mode control (STSMC), a variant of the sliding mode control (SMC), is an effective approach employed in wind energy systems for providing smooth power transfer, robustness, inherent chattering suppression and error-free control. The STSMC has certain disadvantages of (a) less anti-disturbance capabilities due to the non-linear part that is based on variable approaching law and (b) time delay created by the disturbance and uncertainties. This paper enhances the anti-disturbance capabilities of STSMC by combining the attributes of artificial intelligence with STSMC. Initially, the STSMC is designed for both the inner and outer loop of a doubly fed induction generator (DFIG) based wind energy conversion system (WECS). Then, an artificial neural network (ANN)-based compensation term is added to improve the convergence and anti-disturbance capabilities of STSMC. The proposed ANN based STSMC paradigm is validated using a processor in the loop (PIL) based experimental setup carried out in Matlab/Simulink.

INDEX TERMS Sliding mode control, wind energy, super-twisting, artificial intelligence.

I. INTRODUCTION

The high penetration of renewable energy (RE) power generation system in the power grid has decreased the consumption of fossil fuels, evident from the decrease of 81 % in 2016 that was 86 % in 1973 [1]. Major part in this RE integration is played by the wind energy. The wind energy is transferred to the main grid through a composite system called as wind energy conversion system (WECS) that consists of wind turbine, generator, gear box, and control equipment. The power electronics are used to integrate the generated electricity into the utility grid after the wind energy is converted to electricity by the WECS [2]. The rapid advancement of power converters has resulted in the WECS getting smaller and less expensive [4], [5], [6], [7].

Control of WECS is critical in renewable energy technologies. Various generators are used in WECS having complex structures and highly nonlinear dynamics. Such a highly nonlinear system needs robust control to tackle external disturbances, nonlinearities, and uncertainties. Sliding mode control (SMC), widely known as variable structure control, is a good solution that meets the requirements of WECS.

The associate editor coordinating the review of this manuscript and approving it for publication was Anandakumar Haldorai.

TABLE 1. Nomenclature.

ρ	Air density	R	Wind turbine rotor radius
v	Wind speed	$C_p(\lambda, \beta)$	Power coefficient
λ	Tip speed ratio	β	Pitch angle
ω_t	Turbine shaft angular speed	$k_1, k_2,, k_3, k_4$	Positive constants
G	Gear ratio	ω_r	Generator speed
T_r	Generator torque	T_t	Aerodynamic torque
I_{ds}, I_{qs}	Stator (dq) currents	L_s, L_r	Stator and rotor inductance
L_m	Stator mutual inductance	R_s, R_r	Stator and rotor resistance
E	DC Link Voltage	p	Number of pole pairs
ω_r and ω_s	Rotor and stator angular speed	$\varphi_{ds}, \varphi_{qs}$	Rotor (dq) fluxes
V_{ds}, V_{qs}	Stator (dq) voltages	T_{em}	Electromagnetic torque
f_r	Viscous friction coefficient	J	Moment of inertia
T_L	Load torque	P_s	Active power
Q_s	Reactive Power	ω_r^{ref}	reference generator speed
$\mathfrak{S}$	sliding surface	P_{grid}^{ref}	the reference grid power
V_{gd}, V_{gq}	grid (dq) voltages	$(\alpha, \beta)_\omega, (\alpha, \beta)_{1,2}, (\alpha, \beta)_E$	Positive constants

Classical SMC is a power control method widely used in WECS. The most fundamental and straightforward control design for DFIG-based WECS is the first order SMC. A good compromise between torque oscillations and the effectiveness of power conversion is offered by the SMC. The surface for the first order SMC, proposed in [8], is selected as the error between reference power and actual power. For frequency change under sudden load conditions, the reference power is chosen to be less than the maximum power. The suggested scheme is verified using a test bench created at NREL FAST. For grid-connected WECS, a similar idea has been introduced in [9] and [10]. The previously mentioned first-order SMC schemes are continuous. The SMC based control schemes inherit an undesirable phenomenon of chattering and proved it to be harmful to the system as stated by Utkin and Lee [11], that results in high wear and tear, excessive power losses, and low control accuracy of the system. This phenomenon is due to the discontinuous switching control law in the continuous control schemes. Instead of a constant reaching law, the author in [12] proposes an exponential reaching law to solve the chattering issue. The exponential reaching law-based SMC gains are scheduled in accordance with the error magnitude. The gain increases as the error increases, and decreases as the error decreases. According to [12], the enhanced reaching law is expressed as follows:

$$\dot{\mathfrak{S}} = -\Lambda\mathfrak{S} - \frac{Q}{D(\mathfrak{S})}|\mathfrak{S}|^{\gamma_x}\,\text{sign}(\mathfrak{S}) \tag{1}$$

where

$$D(\mathfrak{S}) = \alpha + (1-\alpha)e^{-\beta_x|\mathfrak{S}|}$$

and $0 < \alpha < 1$ and $\beta_x > 0$. It is evident from the surface equation given above, that the gain modification is performed between $Q|\mathfrak{S}|^{\gamma_x}$ and $Q|\mathfrak{S}|^{\gamma_x}/\alpha$,as per the magnitude of error. Digital control schemes are also introduced to enhance the SMC schemes. In order to implement a switching-free control strategy, digital sliding mode control (DSMC) based on the adaptive reaching law was first presented in [13] by Milosavljević. The authors introduced the concept of quasi-sliding mode (QSM), where the system's trajectory is along a surface that produces motion similar to sliding rather than switching surfaces. The digitalized SMC guarantees to slide at each sampling instant [14], [15]. The digital SMC are further studied and elaborated in [13] and [16]. Other enhancement techniques use approximation of signum function using sigmoid function or continuous saturation function [17] for chattering elimination at the expense of system robustness. A new family of classical SMC was proposed to reduce the chattering known as boundary layer SMC, whereas the terminal SMC concept has been used to provide finite-time convergence. Another variant of SMC known as second-order SMC (SOSMC) is a successful technique in removing the shortcomings of SMC (i.e., chattering and infinite-time convergence) while retaining the inherent robust nature of the classical SMC [18]. A high order sliding mode control using a super-twisting algorithm (STA) has been proposed by [19] for wind energy systems. The STA-based SMC schemes are easy to implement and this is implemented to make the wind energy systems more robust. Various variants of super-twisting SMC (STSMC) are also reported in the literature. For instance, the author in [20] combines the STSMC and fractional order calculus to improve the performance of the system with a chattering elimination approach. The author in [21] uses a novel optimization method with STSMC for a direct torque-controlled wind energy system and minimizes the ripples in the torque and flux. The literature depicts that STSMC has certain advantages of chattering elimination, finite-time convergence, no knowledge of perturbations for a system of relative degree one, continuous nature, and ensures robustness against Lipschitz continuous disturbance having bounded gradients.

Although the STSMC improves the system performance, it has certain drawbacks under disturbing scenarios. The standard STSMC having fixed gains is not capable of handling the uncertainties and disturbances growing with the state variable or with time due to the homogeneous nature of the STSMC

scheme [22]. Several efforts have been made to improve the performance of standard STSMC for timely growing uncertainties. The performance of STSMC has been improved by using variable gains. The variable gains were initially introduced to the first order SMC applied under the perturbations with known bounds *a priori* [23], [24]. The same concept was also applied in [25] with a non-homogeneous control structure and timely growing correction terms. This concept has been employed to improve the performance of wind energy conversion systems. For instance, the authors in [26] and [27] proposed the STSMC scheme based on the variable gain structure proposed in [25] and achieved rare output chattering, maximized power, low stress, and smoother firing angles of converters. The variable gain STSMC has further been modified using fuzzy logic theory [28], ANFIS [29], and barrier function [30] for wind energy systems. Although, these variations in standard STSMC improve the performance, but increases the mathematical and computation complexities of the applied control schemes. Artificial intelligence techniques that include deep reinforcement learning and feedforward techniques are also employed to update the weights of the STSMC scheme as reported in [31], [32], and [33]. These techniques serve as adaptive control schemes and improve the performance of STSMC, and at the same time adding more complexity to the system. To assess this situation and improve the performance of STSMC scheme, this paper introduces the artificial intelligence with STSMC paradigm for DFIG-based wind energy systems. The proposed AI based STSMC (AISTSMC) system shown in Fig. 1, which results in the following major contributions:

- The SMC is enhanced using super-twisting SMC scheme. The problems generated from using high order control schemes are evaluated theoretically and mathematically. The non-linear part that is based on the variable approaching law lacks the anti-disturbance capability. This may result in system inability to follow the ideal trajectory and convergence delay. Thus, a new controller is then synergized with STSMC to cope with the aforementioned problems.
- A new AISTSMC technique is proposed using artificial neural network to reduce the tracking error and improve the convergence trajectory of STSMC scheme. The new control law adequately compensates the highly non-linear internal and external disturbances, modeling errors, and parametric uncertainties. The disadvantages of STSMC are convergence delay due to uncertainty and degraded transient performance, which are addressed using AISTSMC scheme.
- The proposed strategy exhibits improved performance, validated through extensive numerical simulations and experimental environment based on processor in the loop (PIL) concept. The results are numerically presented and compared with conventional SMC and STSMC schemes for chattering elimination and robustness against disturbances of step and stochastic nature.

II. SYSTEM DYNAMICS OF DFIG-WECS

The implementation of SMC law utilizes the dynamic model of DFIG-based WECS. The DFIG-based WECS comprises a hub, low and high-speed shafts, gearbox, brake, and a generator. The model order is determined by the number of joints or degrees of freedom; thus, a two-mass model is adopted in this paper. The aerodynamic power from the wind speed is given as follows:

$$P = \frac{1}{2}\rho\pi R^2 C_p(\lambda, \beta)v^3 \quad \text{where} \tag{2}$$

$$\lambda = \frac{\Omega_t R}{v} \tag{3}$$

$$C_p = c_1\left(\frac{c_2}{\lambda} - 1\right)e^{\frac{-c_3}{\lambda}} \tag{4}$$

At $\lambda = \lambda_{opt}$, the C_p reaches its maximum value, thus $C_p = C_{p-\max}$. In this case, the torque of the wind turbine is as follows:

$$T_r = \frac{T_t}{G}\omega_t = \frac{\omega_r}{G} \tag{5}$$

The reference generator speed is given as follows:

$$\omega_r^{ref} = \frac{\lambda_{opt} G}{R}v \tag{6}$$

The reference speed is calculated using (6) when the system is operating at maximum power point, whereas, it is calculated from power curve data and look up tables in other cases. The reference grid power is given as follows:

$$P_{\text{grid}}^{ref} = \frac{1}{2}\eta\rho\pi^2 C_{p-\max}v^3 \tag{7}$$

$$\left.\begin{aligned} V_{ds} &= R_s I_{ds} + \frac{d}{dt}\varphi_{ds} - \omega_s\varphi_{qs} \\ V_{qs} &= R_s I_{qs} + \frac{d}{dt}\varphi_{qs} + \omega_s\varphi_{ds} \\ V_{dr} &= R_r I_{ds} + \frac{d}{dt}\varphi_{dr} - (\omega_s - \omega_r)\varphi_{qs} \\ V_{qr} &= R_r I_{qs} + \frac{d}{dt}\varphi_{qr} - (\omega_s - \omega_r)\varphi_{ds} \end{aligned}\right\} \tag{8}$$

The rotor dynamics of DFIG is given by:

$$J\frac{d}{dt}\omega_r = T_{em} - T_r - f_r\omega_r \tag{9}$$

where the electromagnetic torque is given as follows:

$$T_{em} = P\frac{MV_s}{\omega_s L_s}\left(\varphi_{qs}I_{dr} - \varphi_{ds}I_{qr}\right) \tag{10}$$

As per the concept of vector control, aligning the reference frame to the d-axis of stator flux one gets $\varphi_{ds} = \varphi_s$ and $\varphi_{qs} = 0$. The electromagnetic torque is given as follows:

$$T_{em} = -P\frac{MV_s}{\omega_s L_s}\varphi_s I_{qr} \tag{11}$$

TABLE 2. SMC techniques applied in literature for WECS.

SMC Technique	Ref. (year)	Errors and Surfaces	System information	Remarks
High Order SMC	[34] (2008)	$\mathfrak{S}_1 = K_{opt}\Omega_e^2 - \frac{3}{2}\frac{P}{2}\phi_{sr} i_q$ $\mathfrak{S}_2 = P_{ref}(t) - \frac{3}{2}\phi_{sr} i_q \omega_e$	PMSG, Rectifier and Inverter, No experimental validation	Two different surfaces are used to control the rectifier using STSMC in order to operate it in the best power conversion and power regulation modes.
	[35] (2012)	$e_\omega = \omega_r^{ref} - \omega_r$ $e_i = I_{rd} - I_{rd}^{ref}$ $\mathfrak{S}_\omega = \omega_r^{ref} - \omega_r$ $\mathfrak{S}_i = I_{rd} - I_{rd}^{ref}$	DFIG, Back-to-back converters, Experimentally validated	The optimal power conversion and power regulation operation modes of the rectifier are controlled using STSMC with two different surfaces.
	[36] (2012)	$e_\omega = \omega_r^{ref} - \omega_r$ $\mathfrak{S}_\omega = \frac{1}{J}\omega_r^{ref} - \Omega_r$	DFIG, No experimental validation	The modified STSMC is based on Lyapunov and has variable gains. Detailed simulations are used to validate the results.
	[37] (2013)	$e_T = T_e^{ref} - T_e$ $e_i = Q_{s,\,ref} - Q_s$ $\mathfrak{S}_T = T_e^{ref} - \frac{3pL_mV_s}{2\omega_s L_s} i_{qr}$ $\mathfrak{S}_i = Q_s^{ref} + \frac{3L_mV_s}{2L_s}\left(i_{dr} - \frac{V_s}{\omega_s L_m}\right)$	DFIG, Back-to-back converters, RSC control, No experimental validation	This paper presents STSMC with variable gains and provides convergence analysis for DFIG-based WECS.
	[38] (2014)	$e_T = T_e^{ref} - T_e$ $e_i = I_{rd} - I_{rd}^{ref}$ $\mathfrak{S}_T = T_e^{ref} - T_e$ $\mathfrak{S}_i = I_{rd} - I_{rd}^{ref}$	DFIG, Back-to-back converters, No experimental validation	A STSMC based second order SMC is presented using FAST code
	[39] (2016)	$e_\omega = \omega_r^{ref} - \omega_r$ $e_E = E^* - E$ $\mathfrak{S}_\omega = \omega_r^{ref} - \omega_r$ $\mathfrak{S}_E = E^* - E$	PMSG, IGBT 8837, Back-to-back converters, Experimentally validated	
	[40] (2017)	$e_i = I_{rdq} - I_{rdq}^{ref}$ $e_E = I_{gdq} - I_{gdq}^{ref}$ $\mathfrak{S}_i = I_{rdq} - I_{rdq}^{ref}$ $\mathfrak{S}_E = I_{gdq} - I_{gdq}^{ref}$	DFIG, Back-to-back converters, RSC and GSC control, No experimental validation	Fuzzy integral terminal theory based STSMC is utilized to present a fault ride through technique.
	[41] (2016)	$\mathfrak{S}_T = T_g^{ref} + T_g$ $\mathfrak{S}_E = Q_g^{ref} - Q_g$	DFIG, Back-to-back converters, No experimental validation	The proposed second order SMC employs a time-varying receding horizon to make it adaptive. After calculating the conservative bounds, an adaptation strategy is suggested.
	[21] (2019)	$e_\varphi = \varphi_r^{ref} - \varphi_r$ $e_T = T_e^{ref} - T_e$ $\mathfrak{S}_\varphi = \varphi_r^{ref} - \varphi_r$ $e_T = T_e^{ref} - T_e$	DFIG, RSC control, No experimental validation	The STSMC gains are best chosen using new rooted tree optimization in the proposed STSMC .
	[42] (2020)	$e_\omega = \omega_r^{ref} - \omega_r$ $\mathfrak{S}_\omega = \dot{e}_\omega + k\, e_\omega$	RSC control (outer loop) No experimental validation	To reduce the chattering phenomenon, a new switching sector-based SMC structure is presented.
	[43] (2019)	$e_\omega = \omega_r^{ref} - \omega_r$ $\mathfrak{S}_\omega = \dot{e}_\omega + k\,\lvert e_\omega\rvert^{\frac{2}{3}} sign(e_\omega)$	RSC control, Experimentally validated	new inertial perturb and observe MPPT method is presented. The STSMC of third order is suggested for speed tracking.
	[44] (2020)	$e_{E1} = (E - E^*)$ $e_{E2} = -\int (E - E^*)dt$ $\mathfrak{S}_E = \lambda e_{E1} + e_{E2}$	PMSG, Rectifier + boost converter + inverter, No experimental validation	To control the DC link voltage in PMSG-based WECS, an SOSMC is presented for the boost converter.
	[45] (2020)	$e_p(t) = P_s^{ref} - P_s$ $e_q(t) = Q_s^{ref} - Q_s$ $\mathfrak{S}_1 = e_p(t)$ $\mathfrak{S}_2 = e_q(t)$	DFIG, RSC control, Experimentally validated	Six power compensation techniques are suggested for improving power quality to a HOSMC.
	[46] (2020)	$e_p = P_s^{ref} - P_s$ $e_q = Q_s^{ref} - Q_s$ $\mathfrak{S}_p = P_s^{ref} - P_s$ $\mathfrak{S}_q = Q_s^{ref} - Q_s$	RSC side control, No experimental validation	Performance is assessed and SMC and STSMC stability analysis are given.
	[47] (2021)	$e_p = P_s - P_s^{ref}$ $e_q = Q_s - Q_s^{ref}$ $\mathfrak{S}_1 = e_p(t)$ $\mathfrak{S}_2 = e_q(t)$	DFIG, RSC control, No experimental, validation	The DFIG WECS is controlled using novel adaptive STSMC paradigm

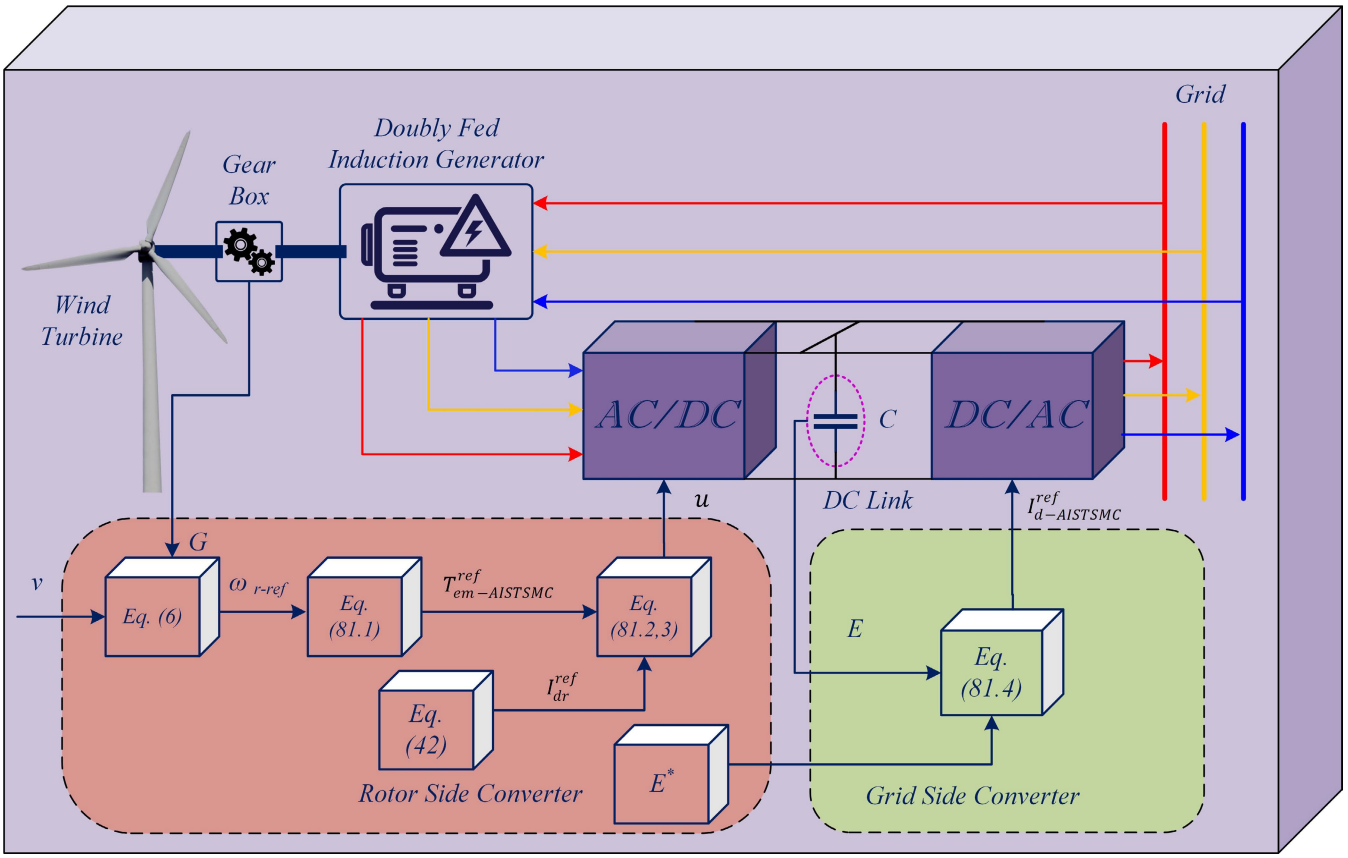

FIGURE 1. DFIG-based WECS operating under proposed control scheme.

The rotor currents, active and reactive power at constant stator flux, $V_{ds} = 0$, and $V_{qr} = V_s = V_{dr} = \omega_s \varphi_s$ are given as follows:

$$\left.\begin{aligned} \tfrac{d}{dt} I_{dr} &= \frac{1}{\sigma L_r}\left(V_{dr} - R_r I_{dr} + s\sigma L_r \omega_s I_{qr}\right) \\ \tfrac{d}{dt} I_{qr} &= \frac{1}{\sigma L_r}\left(V_{q_r} - R_r I_{qr} - s\sigma L_r \omega_s I_{dr}\right) \end{aligned}\right\} \quad (12)$$

$$P_s = -\frac{MV_s}{L_s} I_{qr};\; Q_s = \frac{V_s^2}{\omega_s L_s} I_{qr} - \frac{MV_s}{L_s} I_{dr} \quad (13)$$

A. GRID MODEL

The grid side model in terms of grid voltages, currents, and grid parameters are given as follows:

$$\left.\begin{aligned} V_{gd} &= \omega_g L_g i_{gq} - L_g \tfrac{d}{dt} I_{gd} + e_d - R_g I_{gd} \\ V_{gq} &= -\omega_g L_g i_{gd} - L_g \tfrac{d}{dt} I_{gq} + e_q - R_g I_{gq} \end{aligned}\right\} \quad (14)$$

Rearranging the above equations, one gets the grid model in terms of current dynamics:

$$\left.\begin{aligned} \frac{d}{dt} I_{gd} &= \frac{1}{L_g}\left(e_d - R_g I_{gd} - V_{gd} + \omega_g L_g I_{gq}\right) \\ \frac{d}{dt} I_{gq} &= \frac{1}{L_g}\left(e_q - R_g I_{gq} - V_{gq} - \omega_g L_g I_{gd}\right) \end{aligned}\right\} \quad (15)$$

The DFIG rotor experiences a dynamic and variable wind flow as a result of the wind's stochastic and gusty nature. Therefore, it is necessary to an effective paradigm should be implemented to complete the challenging task of regulating a constant DC link voltage. To accomplish this task, a vector control strategy will be used. The orientation of reference frame is aligned with grid or stator voltage using the vector control strategy. Thus when $V_S = V_D$ and $V_Q = 0$, active power and reactive power adapts a new structure given as:

$$\left.\begin{aligned} P_g &= \frac{3}{2}\left(V_{gd} I_d + V_{gq} I_{gq}\right) = \frac{3}{2}\left(V_{gd} I_d\right) \\ Q_g &= \frac{3}{2}\left(V_{gq} I_{gd} + V_d I_{gq}\right) = \frac{3}{2}\left(V_{gd} I_{gq}\right) \end{aligned}\right\} \quad (16)$$

As shown in (16), I_d and I_q directly impacts the flow of electric power from grid to the converters that equalizes to the DC power given as follows:

$$I_{os} = \frac{3}{2E} V_{gd} I_{gd} \quad (17)$$

$$C\frac{dE}{dt} = I_{os} - I_{or} \quad (18)$$

Substituting (17) in (18), we get:

$$\dot{E} = g(x) I_{gd} - \tfrac{1}{c} I_{or} \quad \text{where} \quad g(x) = \frac{1}{c}\frac{3}{2E} V_{gd} \quad (19)$$

The uncertain term $\Delta g(x)$ is added to $g(x)$ in (19),and is given as follows:

$$g(x) = g_0(x) + \Delta g(x); \quad g_o(x) = \frac{1}{c}\frac{3}{2E_{ref}}V_{gd} \tag{20}$$

where E_{ref} is the reference value of E. Putting $g(x)$ from (20) in to (19), it gives us:

$$\dot{E} = g_0(x)I_{gd} - \frac{1}{c}I_{or} + dE; \quad dE = \Delta g(x)I_{gd} \tag{21}$$

III. PROBLEM FORMULATION AND DESIGN OF STANDARD STSMC

This section initially formulates the mathematical model of DFIG-WECS for developing the problems in the system due to non-linear uncertainties. Various controllers have been developed and discussed in this section to mitigate the problems arising from uncertainties and perturbation.

A. STATE SPACE MODELING AND PROBLEM FORMULATION

The classical linear controllers have satisfactory performance in linear time-varying systems. Contrary, the DFIG is a highly non-linear and strongly coupled system and becomes more complex when operated in grid-connected mode. The varying operating and environmental conditions make the control more difficult. A robust non-linear control system like SMC is necessary for the efficient control of the DFIG-based wind energy systems under both normal and disturbed conditions. The SMC principle is to bring a system to the proposed sliding surface with a non-linear control law consisting of a switching function resulting in the gradual stabilization to the equilibrium point of the system on that surface. The DFIG-based non-linear system needs to be represented in state space form along with the uncertain dynamics to understand, design, and improve the SMC design. The non-linear system given in section II is represented as follows in its state space form:

$$\dot{x}(t) = F(x) + G(x)u \tag{22}$$

The states and the non-linear dynamic function $F(x)$ and $G(x)$ are given as follows:

$$x(t) = \begin{bmatrix} x_1 & x_2 & x_3 \end{bmatrix}^T = \begin{bmatrix} \omega_r & i^r_{qs} & i^r_{ds} \end{bmatrix}^T \tag{23}$$

$$F(x) = \begin{bmatrix} F_\omega \\ F_q \\ F_d \end{bmatrix} = \begin{bmatrix} -(1/J)(T_r + f_r\Omega_r) \\ -\dfrac{R_r}{\sigma L_r}I_{dr} + s\omega_s I_{qr} \\ -\dfrac{R_r}{\sigma L_r}I_{qr} - s\omega_s I_{dr} - s\dfrac{MV_s}{\sigma L_r L_s} \end{bmatrix} \tag{24}$$

$$G(x) = \begin{bmatrix} G_\omega & 0 & 0 \\ 0 & G_q & 0 \\ 0 & 0 & G_d \end{bmatrix} = \begin{bmatrix} \dfrac{1}{J} & 0 & 0 \\ 0 & \dfrac{1}{\sigma L_r} & 0 \\ 0 & 0 & \dfrac{1}{\sigma L_r} \end{bmatrix} \tag{25}$$

$$u = \begin{bmatrix} T_{em} & V_{qr} & V_{dr} \end{bmatrix}^T \tag{26}$$

Once the system is defined in the desired state, the control objective is defined. In the presence of system uncertainties and disturbances, the control objective is the convergence of the current state vector to the desired or reference state vector. For this purpose, a sliding variable $\mathfrak{S}$ is designed to achieve the required dynamic of the system given in (22) during the sliding mode $\mathfrak{S} = \mathfrak{S}(x,t) = 0$. Also, it is assumed that the relative degree of the input-output ($u \rightarrow \mathfrak{S}$) is one, with stable internal dynamics. Therefore, the input-output dynamics can be presented as:

$$\dot{\mathfrak{S}} = \underbrace{\frac{\partial s}{\partial t} + \frac{\partial s}{\partial x}F(x)}_{\mathfrak{F}(x,t)} + \underbrace{\frac{\partial s}{\partial x}G(x)u}_{\mathfrak{G}(x,t)} \tag{27}$$

Also, it is assumed that:

A1: The uncertain function $\mathfrak{G}(x,t) \in R$ exists and can be shown as follows:

$$\mathfrak{G}(x,t) = \mathfrak{G}_0(x,t) + \Delta\mathfrak{G}(x,t) \tag{28}$$

where $\mathfrak{G}_0(x,t) > 0$ is a function that is known and $\Delta\mathfrak{G}(x,t)$ is a bounded uncertainty so that

$$\frac{|\Delta\mathfrak{G}(x,t)|}{\mathfrak{G}_0(x,t)} = \varrho(x,t) \leq \varrho_1 < 1 \tag{29}$$

$\forall x \in R^n$ and $t \in [0,\infty)$ with an unknown boundary ϱ_1.

A2:. The function $\mathfrak{F}(x,t) \in R$ is presented as

$$\mathfrak{F}(x,t) = \mathfrak{F}_1(x,t) + \mathfrak{F}_2(x,t) \tag{30}$$

with the bounded terms

$$\left.\begin{aligned} |\mathfrak{F}_1(x,t)| &\leq \delta_1|s|^{1/2} \\ |\mathfrak{F}_2(x,t)| &\leq \delta_2 \end{aligned}\right\} \tag{31}$$

where the finite boundaries $\delta_1, \delta_2 > 0$ exist but is unknown. A final equation is given is follows:

$$\dot{\mathfrak{S}} = \mathfrak{F}(x,t) + \underbrace{\left(1 + \underbrace{\frac{\Delta\mathfrak{G}(x,t)}{\mathfrak{G}_0(x,t)}}_{\mathfrak{G}_2(x,t)}\right)}_{\mathfrak{G}_1(x,t)}\mu \tag{32}$$

where $\mu = \mathfrak{G}_0(x,t)u$. From A1, one gets

A3:

$$1 - \varrho_1 \leq \mathfrak{G}_1(x,t) \leq 1 + \varrho_1 \tag{33}$$

The objective now is to drive the sliding surface $\mathfrak{S}$ and $\dot{\mathfrak{S}}$ to zero under disturbance and perturbations in finite-time. SMC can efficiently fulfill this objective when the boundary of the disturbance is known.

B. FIRST ORDER SMC DESIGN FOR DFIG-WECS

The surfaces that will be used in the design of first-order SMC are selected as an error between the reference and actual states. The surfaces are suggested based on the difference between the reference and the state variable. In DFIG-based WECS, the controllable state components include current, speed, and DC link voltage. These controllable state components will be used to control the WECS in this section.

C. ROTOR SIDE CONTROL

1) SPEED CONTROL

The speed control is the first step to in the RSC control, where speed error is taken given as follows:

$$e_\omega = \omega_r - \omega_r^{ref} \tag{34}$$

Taking its derivative as $\dot{e}_\omega = \dot{\omega}_r - \dot{\omega}_r^{ref}$; and putting the values from (9) we have:

$$\dot{e}_\omega = \frac{T_{em}}{J} + d_3 - \dot{\omega}_r^{ref} \tag{35}$$

The surface is selected as (35) and is given as follows:

$$\mathfrak{S}_\omega = e_\omega \tag{36}$$

Taking derivative of the above surface, one gets the following relation:

$$\dot{\mathfrak{S}}_\omega = \dot{e}_\omega = \frac{T_{em}}{J} + d_3 - \dot{\omega}_r^{ref} \tag{37}$$

The SMC law consists of an equivalent terms which is acquired here by selecting $\dot{\mathfrak{S}}_\omega = 0$. The equivalent term is given as follows:

$$T_{em}^{eq} = J\left(\dot{\omega}_r^{ref} - d_3\right) \tag{38}$$

The final control law T_{em-SMC}^{ref} is obtained using T_{em}^{eq} in (38) and switching control part $T_{em}^{s} = -J(k_3\,\mathrm{sgn}(\mathfrak{S}_\omega))$ and is given as follows:

$$\left.\begin{aligned} T_{em-SMC}^{ref} &= T_{em}^{eq} + T_{em}^{s} \\ T_{em}^{eq} &= J\left(\dot{\omega}_r^{ref} - d_3\right) \\ T_{em}^{s} &= -J\,(k_3\ \ \mathrm{sgn}\,(\mathfrak{S}_\omega)) \end{aligned}\right\} \tag{39}$$

2) CURRENT CONTROL

The objective of current control law derivation is to ensure the current x tracking of x^{ref} where the x^{ref} is given as follows:

$$x^{ref} = [I_{dr}^{ref} \quad I_{qr}^{ref}]^T \tag{40}$$

The reference $q-$axis current (I_{qr}^{ref}) is obtained from(11) and is given as follows:

$$I_{qr}^{ref} = \frac{\omega_s L_s}{PMV_s} T_{em}^{ref} \tag{41}$$

The d-axis reference current is derived by substituting $Q_s^{ref} = 0$, in reference reactive power $Q_s^{ref} = \frac{V_s^2}{\omega_s L_s} - \frac{MV_s}{\omega_s L_s} I_{dr}$ and is given as:

$$I_{dr}^{ref} = \frac{V_s}{\omega_s M} \tag{42}$$

The current control is the second step to in the RSC control that takes the reference current from speed control loop and uses the current error, given as follows:

$$\left.\begin{aligned} e_i &= x - x^{ref} \\ e_i &= [e_1 \quad e_2]^T \\ e_i &= \left[I_{dr} - I_{dr}^{ref} \quad I_{qr} - I_{qr}^{ref}\right] \end{aligned}\right\} \tag{43}$$

The next step is to take the derivative of current errors given in (43). The values of variables are substituted in derivatives of current errors from (12) and are given as follows:

$$\left.\begin{aligned} \dot{e}_1 &= \frac{1}{\sigma L_r}(V_{dr} - R_r I_{dr} + s\sigma L_r \omega_s I_{qr} - \dot{I}_{dr}^{ref} \\ \dot{e}_2 &= \frac{1}{\sigma L_r}(V_{qr} - R_r I_{qr} + s\sigma L_r \omega_s I_{dr} - \dot{I}_{qr}^{ref} \end{aligned}\right\} \tag{44}$$

Hence (44) can be written as:

$$\left.\begin{aligned} &\left.\begin{aligned} \dot{e}_1 &= G_1 + \frac{1}{\sigma L_r} V_{dr} - \frac{1}{\sigma L_r} R_r I_{dr} \\ \dot{e}_2 &= G_2 + \frac{1}{\sigma L_r} V_{qr} - \frac{1}{\sigma L_r} R_r I_{qr} \end{aligned}\right\} \\ &\text{where} \left\{\begin{aligned} G_1 &= \frac{1}{\sigma L_r}(s\sigma L_r \omega_s I_{qr} - \dot{I}_{dr}^{ref}) \\ G_2 &= \frac{1}{\sigma L_r}(s\sigma L_r \omega_s I_{dr} - \dot{I}_{qr}^{ref}) \end{aligned}\right. \end{aligned}\right\} \tag{45}$$

The current control loop derivation is performed by selecting the surface same as the dq current errors, given as follows:

$$\mathfrak{S} = \begin{bmatrix} \mathfrak{S}_1 \\ \mathfrak{S}_2 \end{bmatrix} = \begin{bmatrix} e_1 \\ e_2 \end{bmatrix} \tag{46}$$

The derivative of the above surface is given as follows:

$$\dot{\mathfrak{S}} = \begin{bmatrix} \dot{\mathfrak{S}}_1 \\ \dot{\mathfrak{S}}_2 \end{bmatrix} = \begin{bmatrix} \dot{e}_1 \\ \dot{e}_2 \end{bmatrix} \tag{47}$$

Selecting $\dot{\mathfrak{S}} = 0$, and the using the SMC theory, a final current control law consisting of equivalent control and discontinuous control terms is derived given as follows:

$$\left.\begin{aligned} V_{dr-SMC}^{ref} &= \sigma L_r(\underbrace{\frac{R_r}{\sigma L_r} I_{dr} - G_1}_{V_{dr}^{eq}} - k_1\,\mathrm{sgn}\,(\mathfrak{S}_1)) \\ V_{qr-SMC}^{ref} &= \sigma L_r(\underbrace{\frac{R_r}{\sigma L_r} I_{qr} - G_2}_{V_{qr}^{eq}} - k_2\,\mathrm{sgn}\,(\mathfrak{S}_2)) \end{aligned}\right\} \tag{48}$$

here V_{dr}^{ref} and V_{qr}^{ref} are the references voltages to be fed to modulation stage.

D. GRID SIDE CONTROL

The third step in the control of DFIG-WECS is DC link voltage control scheme derivation, that is performed by taking the DC link voltage error e_E shown as below:

$$e_E = E - E_{ref} \tag{49}$$

Now, to get the final control law, derivative of voltage error is first taken and then values from (21) are substituted to get the following equations:

$$\left.\begin{aligned} \dot{e}_E &= \dot{E} - \dot{E}^{ref} \\ \dot{e}_E &= g_0(x) I_{gd} - \frac{1}{C} I_{or} + dE - \dot{E}_{ref} \end{aligned}\right\} \tag{50}$$

Now selecting the surface for GSC control law same as the voltage error given as follows:

$$\mathfrak{S}_E = e_E \tag{51}$$

The derivative of the surface for GSC control law is given as:

$$\dot{\mathfrak{S}}_E = \dot{e}_E \tag{52}$$

Now using the SMC theory, the equivalent part is derived from above equation equalizing to zero, and taking the discontinuous term as $I_{d-s} = \frac{1}{g_0(x)}(-k_4 \operatorname{sgn}(\mathfrak{S}_E))$, the following control is obtained:

given

$$\left.\begin{aligned} I_{d-SMC}^{ref} &= I_{d-eq} + I_{d-s} \\ I_{d-eq} &= \frac{1}{g_0(x)}\left(\dot{E}^{ref} + \frac{1}{C} I_{0r}\right) \\ I_{d-s} &= \frac{1}{g_0(x)}(-k_4 \operatorname{sgn}(\mathfrak{S}_E)) \end{aligned}\right\} \tag{53}$$

The control laws for RSC and GSC derived in the above section can improve the performance of DFIG-WECS but it can also result in degraded performance due to the inherent chattering. A number of techniques are present in literature to attenuate the chattering phenomenon in which high order sliding mode control (HOSMC) schemes are widely adapted. A type of HOSMC known as STSMC can successfully eliminate the chattering phenomenon.

E. SUPER-TWISTING SMC DESIGN FOR DFIG-WECS AND LIMITATIONS

The sliding mode control is divided into five generations, according to Fridman *et al.* [48] (1) first Sliding mode control, super-twisting algorithms, arbitrary order SMC, and continuous arbitrary SMC. The third-generation STSMC benefits from Lipschitz uncertainties with control signal of a continuous type. For WECS, the authors of [49], [50], [51], [52], [53], [54], and [55] proposed STSMC. The HOSMC maintains the benefits of the FOSMC, such as invariance and robustness, chattering elimination and control accuracy improve by removing the relative degree limitations [56]. The simplified structured super-twisting algorithm (STA), which requires least target information, is the most widely used algorithm for achieving HOSMC [57], [58]. The control law is deduced here using the STA structure described in [38].

$$\left.\begin{aligned} u &= \frac{1}{\mathfrak{G}_o}\left[-\mathfrak{F}(x,t) + \mu_1 + \mu_2\right] \\ \mu_1 &= -\alpha\sqrt{|\mathfrak{S}(t)|}\operatorname{sign}(\mathfrak{S}(t)) \\ \dot{\mu}_2 &= -\frac{\beta}{2}\operatorname{sign}(\mathfrak{S}(t)) \end{aligned}\right\} \tag{54}$$

where the bounded control gains, α and β, are determined by the system's operating under unknown disturbances. Using the attributes of STSMC, a speed control is derived using the STA and equivalent term from (39). The STSMC based control paradigm is given as follows:

$$\left.\begin{aligned} T_{em-STSMC}^{ref} &= T_{em-eq} + T_{em-s} \\ T_{em-eq} &= J\left(\dot{\omega}_r^{ref} - d_3\right) \\ T_{em-s} &= J\left(-\alpha_\omega |\mathfrak{S}_\omega|^{\frac{1}{2}} \operatorname{sign}(\mathfrak{S}_\omega) - \beta_\omega \int \operatorname{sign}(\mathfrak{S}_\omega)\right) \end{aligned}\right\} \tag{55}$$

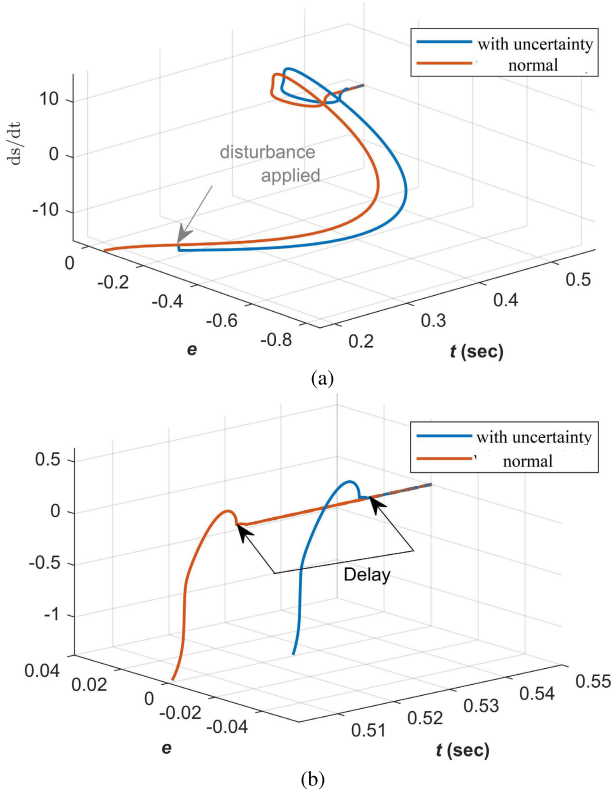

FIGURE 2. STSMC trajectory comparison under normal and disturbed conditions. (a) Normal view. (b) Zoomed view portraying delay in the system trajectory.

In the similar way, the STA (54) and the equivalent part in (48) are used to obtain the RSC control law given as follows:

$$\left.\begin{aligned} V_{dr-STSMC}^{ref} &= \sigma L_r(\underbrace{\frac{R_r}{\sigma L_r} I_{dr} - G_1}_{V_{dr}^{eq}} - \alpha_1 |\mathfrak{S}_1|^{\frac{1}{2}} \operatorname{sign}(\mathfrak{S}_1) \\ &\quad - \beta_1 \int \operatorname{sign}(\mathfrak{S}_1)) \\ V_{qr-STSMC}^{ref} &= \sigma L_r(\underbrace{\frac{R_r}{\sigma L_r} I_{qr} - G_2}_{V_{qr}^{eq}} - \alpha_2 |\mathfrak{S}_2|^{\frac{1}{2}} \operatorname{sign}(\mathfrak{S}_2) \\ &\quad - \beta_2 \int \operatorname{sign}(\mathfrak{S}_2)) \end{aligned}\right\} \tag{56}$$

To transfer power from RSC to grid, the GSC employs the same surface made up of the difference between the DC link voltage and its reference. The new HOSMC law for GSC using (54) and equivalent law from (53) is given as follows:

$$\begin{aligned} I_{d-STSMC}^{ref} = \frac{1}{g_0(x)}\Bigg[&\dot{E}^{ref} + \frac{1}{C} I_{0r} - \alpha_E |\mathfrak{S}_E|^{\frac{1}{2}} \operatorname{sign}(\mathfrak{S}_E) \\ &- \beta_E \int \operatorname{sign}(\mathfrak{S}_E)\Bigg] \end{aligned} \tag{57}$$

The DFIG-based WECS is prone to certain uncertainties. The ideal convergence trajectory cannot be achieved under these uncertainties. The STSMC law consists of two components: (1) integral part $-\frac{\beta}{2}\int sign(\mathfrak{S}(t))dt$ and nonlinear part

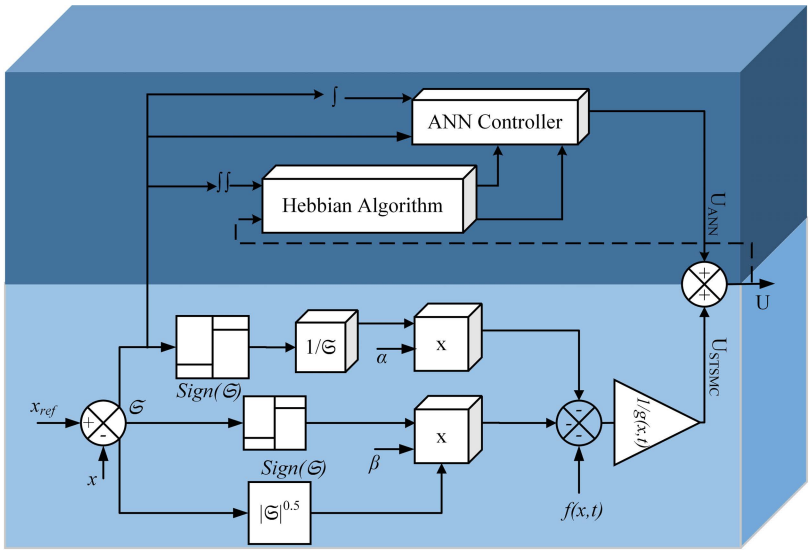

FIGURE 3. Proposed AISTSMC based control scheme.

$-\alpha\sqrt{|\mathfrak{S}(t)|}sign(\mathfrak{S}(t))dt$. The non-linear part that is based on variable approaching law lacks the ant-disturbance capability. Thus, under the disturbed condition, the system cannot follow the ideal trajectory resulting in convergence delay as shown in Fig. 2. The convergence delay based on the analysis of [24] is given as t_B in the following equation:

$$\left.\begin{aligned} t_0 &< t_A + t_B \\ t_A &= \frac{2\sqrt{e(0)\,|}}{\alpha} \\ t_B &= \frac{\Delta\mathfrak{G}(0) + \left(\beta + |\Delta\widehat{\dot{\mathfrak{G}}}|\right) t_A}{\beta - |\Delta\dot{\mathfrak{G}}|} \end{aligned}\right\} \tag{58}$$

where, t_B can be seen as the convergence delay cause by the system disturbance. The trajectory of the STSMC scheme under normal and uncertain situation is shown in Fig. 2 that clearly shows the convergence delay. The asymptotic stability of STSMC control scheme using Lyapunov stability theorem is given as under:

$$\left.\begin{aligned} \dot{V} &= \mathfrak{S}^T \cdot \dot{\mathfrak{S}} \\ \dot{V} &= \mathfrak{S}^T \left(-\alpha\sqrt{|\mathfrak{S}|}\,\mathrm{sgn}(\mathfrak{S}) - \int \beta\,\mathrm{sgn}(\mathfrak{S})dt + \Delta\mathfrak{G}(t)\right) \\ \dot{V} &= -\mathfrak{S}^T\alpha\sqrt{|\mathfrak{S}|}\,\mathrm{sgn}(\mathfrak{S}) - \mathfrak{S}^T \int \beta\,\mathrm{sgn}(\mathfrak{S})dt + \mathfrak{S}^T\Delta\mathfrak{G}(t) \end{aligned}\right\} \tag{59}$$

Putting the value of $sgn = \frac{\mathfrak{S}}{|\mathfrak{S}|} = \frac{|\mathfrak{S}|}{\mathfrak{S}}$ in the above expression, one gets:

$$\begin{aligned} &\leq -\alpha\left|\mathfrak{S}^T\right|\sqrt{|\mathfrak{S}|} - \left|\mathfrak{S}^T\right|\int \beta dt + \left|\mathfrak{S}^T\Delta\mathfrak{G}(t)\right| \\ &= -\alpha\left|\mathfrak{S}^T\right|\sqrt{|\mathfrak{S}|} - \left|\mathfrak{S}^T\right|\int \beta dt + \left|\mathfrak{S}^T\right|\left|\int \Delta\dot{\mathfrak{G}}(t)dt\right| \\ &\leq -\alpha\left|\mathfrak{S}^T\right|\sqrt{|\mathfrak{S}|} - \left|\mathfrak{S}^T\right|\int \beta dt + \left|\mathfrak{S}^T\right|\int |\Delta\dot{\mathfrak{G}}(t)|dt \end{aligned} \tag{60}$$

where $\Delta\mathfrak{G}(t)$ is uncertainty in the system. Because $|\Delta\dot{\mathfrak{G}}(t)| < \dot{\varrho}_1 < \alpha$, then

$$\begin{aligned} \dot{V} &\leq -\alpha\left|\mathfrak{S}^T\right|\sqrt{|\mathfrak{S}|} - \left|\mathfrak{S}^T\right|\int \beta dt + \left|\mathfrak{S}^T\right|\int \Delta\mathfrak{G}dt \\ &= -\alpha\left|\mathfrak{S}^T\right|\sqrt{|\mathfrak{S}|} - \left|\mathfrak{S}^T\right|\left(\int \beta dt - \int \Delta\mathfrak{G}dt\right) \\ &\leq -\left|\mathfrak{S}^T\right|\sqrt{|\mathfrak{S}|} \\ &\leq 0 \end{aligned} \tag{61}$$

One of the most widely used control methods for WECS has been proved to be STSMC. Table 3 lists the various systems using the STSMC scheme along with their surfaces, errors, and system types. In [49] and [55], the author uses STA to extract the most power possible while maintaining robustness, chatter-free control, finite reaching time, and upper bounds on externally applied disturbances. The authors in [47] have found a solution to the problem with upper bound presumption where an adaptive multivariable control scheme with finite-time convergence and adaptive gain adjustment. To demonstrate the finite-time convergence and stability of the suggested control scheme, a novel Lyapunov stability theory is put forth by [47]. For floating wind turbines, an adaptive super-twisting control scheme has been presented in [59]. In STA algorithm-based control laws, the two controller gains, α and β are fixed and selected to control performance. These gains in each of the aforementioned control laws are typically established by the uncertainties boundary, which depends on several variables. In the process of designing control laws, the uncertainty boundary is typically estimated sufficiently, leading to unnecessary gains. Adaptive sliding mode control (ASMC) schemes are used to address the problems of unnecessary constant gains. The gain is adjusted to be small enough to maintain the sliding motion using ASMC-based schemes that combine SMC theory and adaptive

algorithm characteristics [47]. A recent adaptive STA-based SMC scheme for PMSG-based tidal stream turbine was proposed by Chen *et al.* [60]. The gains listed below can be used to adapt the HOSMC scheme previously mentioned:

$$\dot{\alpha} = \begin{cases} \sigma\sqrt{\gamma_1/2}, & \text{if } \mathfrak{S} \neq 0 \\ 0, & \text{if } \mathfrak{S} = 0 \end{cases}$$
$$\beta = \varepsilon\alpha \tag{62}$$

where γ_1 and ε are positive constants. The adaptive gains given in (62) can sufficiently minimize the chattering and increase the robustness of STSMC scheme, yet the overestimation problem of the adapted gains still persists. The stability proof for the HOSMC can be found in [60] with the Lyapunov function given by [61]. Thus, due to decrease in the robustness of STSMC, an intelligent approach is adapted in this study to enhance the performance of STSMC scheme.

IV. PROPOSED AISTSMC BASED CONTROL SYSTEM

The disadvantages of STSMC discussed in the previous section are convergence delay due to uncertainty and degraded transient performance. A new AISTSMC technique is proposed in this section to reduce the tracking error and improve the convergence trajectory of the STSMC scheme. The new control law consists new term μ_{ANN}, which compensates for the highly non-linear internal and external disturbances, modeling errors, and parametric uncertainties. The artificial neural network and STSMC synergized operation is shown in Fig. 3. The new AISTSMC based control law is given as follows:

$$\mathfrak{u} = u_{eq} + \mu_n + \mu_2 + \mu_{ANN} \tag{63}$$

The AI based part μ_{ANN} in (63) is given as under:

$$\mu_{ANN} = \sum_{i=1}^{k} \beth_i e_i \tag{64}$$

The μ_{ANN} represents the ANN controller with single neuron, adjustable weights, and two inputs. The adjustable weights represented by $\beth_1$ and $\beth_1$ for $i = 1, 2$. The inputs to the ANN controller part are speed, current, and DC link voltage error $E_1 = e$ and their integral $E_2 = \sum_{l=1}^{k} e(i)$. Hebbian algorithm is used to update the adjustable weights represented in implicit scalar form as follows:

$$\dot{\beth} = \beth_i + \eta y(\mathbf{x}) x_i \tag{65}$$

here $y(\mathbf{x}_n)$ is again the output, this time explicitly dependent on its input vector $\mathbf{x}$. The Hebbian algorithm with its input, $\sum_i \beth_i x_i$, followed by a response function $f()$ can be represented as follows:

$$y = f\left(\sum_{i=1}^{N} \beth_i x_i\right). \tag{66}$$

The synaptic weight $\beth_i$ evolution with time is described by Hebbian plasticity as under:

$$\frac{d\beth_i}{dt} = \eta x_i y. \tag{67}$$

The response function y can be represented in a more simpler form is given as under in (68) followed by its version in matrix form in (69):

$$\frac{d\beth_i}{dt} = \eta x_i \sum_{j=1}^{N} \beth_j x_j \tag{68}$$

$$\frac{d\beth}{dt} = \eta \mathbf{x}\mathbf{x}^T \beth. \tag{69}$$

The data variable $\mathbf{x}$ in (69), when taken as an average over continuous (time) or discrete, can be written as:

$$\frac{d\beth}{dt} = \left\langle \eta \mathbf{x}\mathbf{x}^T \beth \right\rangle = \eta < \mathbf{x}\mathbf{x}^T > \mathbf{w} = \eta C \beth. \tag{70}$$

In eigenvectors basis form, $\beth(t)$ is written as follows:

$$\beth(t) = k_1 e^{\eta\alpha_1 t}\mathbf{c}_1 + k_2 e^{\eta\alpha_2 t}\mathbf{c}_2 + \ldots + k_N e^{\eta\alpha_N t}\mathbf{c}_N \tag{71}$$

It is clear from (71) and eigenvectors theory, that one term in (71) dominates others on with the passage of sufficient time and thus:

$$\beth(t) \approx e^{\eta a^* t}\mathbf{c}^* \tag{72}$$

where α^* is the largest eigenvalue of C. The postsynaptic neuron performs the following operation at this instant:

$$y \approx e^{\eta\alpha^* t}\mathbf{c}^*\mathbf{x} \tag{73}$$

The largest eigenvalue $\mathbf{c}^*$ is related to the computation of first principal component. Hebbian algorithm using the double integrated values of the error is used to tune the weights $\tilde{\beth}_i$ making it adaptive. The adaptive weights are given as follows:,

$$\dot{\tilde{\beth}}_i = \tilde{\beth}_i + \eta_i Z_i U \tag{74}$$

where , $Z_i = \int_{n=1}^{k}\int_{n=1}^{k} e, U$ is the control signal, and η_i is the learning rates. Equation (74) is implemented using discontinuous projector operator shown as follows:

$$\tilde{\beth}_i = proj\tilde{\beth}\left[\zeta\tilde{\beth}_i\right] \tag{75}$$

where ζ represents the learning gain. The projection operator is defined as follows:

$$proj_{\tilde{\beth}_i}(\star) = \begin{bmatrix} 0 & \text{if } \tilde{\beth}_i = \beth_{i\max} \text{ and } \star > 0 \\ 0 & \text{if } \tilde{\beth}_i = \beth_{i\min} \text{ and } \star < 0 \\ \star & \text{otherwise} \end{bmatrix} \tag{76}$$

This completes the description and stability analysis of proposed loop synergized with STSMC scheme. Using the μ_{ANN} from (64). The new AISTSMC based control scheme adapts the following structure:

$$\left.\begin{aligned} u_{eq} &= \frac{1}{\mathfrak{G}_o}\left[-\mathfrak{F}(x,t)\right] \\ \mu_n &= -\alpha\sqrt{|\mathfrak{S}(t)|}\,\text{sign}\left(\mathfrak{S}(t)\right) \\ \dot{\mu}_2 &= -\frac{\beta}{2}\,\text{sign}\left(\mathfrak{S}(t)\right) \\ \mu_{AANN}(k) &= \sum_{i=1}^{i=n} \beth_i(k) x_i(k) \end{aligned}\right\} \tag{77}$$

As described earlier, that eh inputs to the ANN controller part are errors $E_1 = e$ and their integral $E_2 = \int ed(t)$, thus (77) can be expanded as follows:

$$\left.\begin{aligned} u_{eq} &= \frac{1}{\mathfrak{G}_o}\left[-\mathfrak{F}(x,t)\right] \\ \mu_n &= -\alpha\sqrt{|\mathfrak{S}(t)|}\,\mathrm{sign}\,(\mathfrak{S}(t)) + \beth_1 e(t) \\ \dot{\mu}_2 &= -\beta\,\mathrm{sign}\,(\mathfrak{S}(t)) + \beth_2 e(t) \end{aligned}\right\} \tag{78}$$

using the relation $e = |e|\,\mathrm{sign}(e)$, the above equation can be further summarized to:

$$\left.\begin{aligned} u_{eq} &= \frac{1}{\mathfrak{G}_o}\left[-\mathfrak{F}(x,t)\right] \\ \mu_n &= (-\alpha + \beth_1\sqrt{|\mathbf{e}|})\sqrt{|\mathfrak{S}(t)|}\,\mathrm{sign}\,(\mathfrak{S}(t)) \\ \dot{\mu}_2 &= (-\beta + \beth_2|\mathbf{e}|)\,\mathrm{sign}\,(\mathfrak{S}(t)) \end{aligned}\right\} \tag{79}$$

Taking $\Theta_\alpha = (\alpha - \beth_1\sqrt{|e|})$, and $\Theta_\beta = (\beta - \beth_2|e|)$, (79) can be written as follows:

$$\left.\begin{aligned} u_{eq} &= \frac{1}{\mathfrak{G}_o}\left[-\mathfrak{F}(x,t)\right] \\ \mu_n &= -\Theta_\alpha\sqrt{|\mathfrak{S}(t)|}\,\mathrm{sign}\,(\mathfrak{S}(t)) \\ \dot{\mu}_2 &= -\Theta_\beta\,\mathrm{sign}\,(\mathfrak{S}(t)) \end{aligned}\right\} \tag{80}$$

The control law in (80) depicts that new ANN based control loop results in a adjustable gain that varies with the error magnitude.

The DFIG-WECS control consists of two major components: rotor side control (RSC) and grid side control (GSC). The main objective in SMC of DFIG-WECS is to track the reference speed in the outer loop of RSC. The error between reference and generator speed is used to generate reference q-axis current. The rotor currents are controlled in the inner control loop of RSC using the error between reference currents and actual currents.

The derivatives of the sliding surfaces given in (36), (46), and (51) when combined with (63) with ANN part in (80) gives the required control law using SMC theory given as in (81), shown at the bottom of the page.

V. PERFORMANCE EVALUATION OF THE PROPOSED CONTROL SCHEMES

This section presents the performance comparison of the proposed AISTSMC with conventional SMC and STSMC schemes through a processor in the loop (PIL) based experimental setup. The PIL-based setup, shown in Fig. 4, uses a Dual Core Processor TMS320F379D integrated with MATLAB/Simulink at a sampling rate of 5×10^{-5} s in discrete time. In the adapted PIL environment, the control board is physically connected to the DFIG-WECS model operating in Simulink. The dual core processor programming is done using rapid prototyping environment from Simulink. The discussed controllers are discretized, and compiled from MATLAB/Simulink and then hex version of these controllers is programmed into the RAM of processor, where data exchange takes place using high speed serial port. Two types of tests are conducted for various control schemes. In the first test, a deterministic wind speed waveform is used as input wind with external disturbance applied as a step load to testify to the robustness of the proposed control scheme. In the second test, a stochastic wind speed waveform is used as input wind. In this test, a lumped uncertainty $d(t)$ commissioning external and parametric uncertainty with 25% variation is added to the DFIG-based WECS. Response optimization is used in this paper to select the SMC and STSMC gains. The Optimization toolbox in MATLAB/Simulink is used to perform the optimization process where integral absolute error has been used as criteria to minimize the objective function. The introduction of ANN to STSMC can cause some problems due to the Hebbian algorithm. The neurons in the ANN controller updated by Hebbian algorithm are activated to increase the weights, that can cause instability. Thus, the weights are normalized in every iteration to limit the infinite increase using the relation $\beth_i'(k) = \beth_i(k)/\sum_{i=1}^{k}|\beth_i(k)|$.

The outcomes of the two case studies considered are explained as follows:

A. CASE 1: PERFORMANCE EVALUATION UNDER STEP UNCERTAINTY

In this test, an external disturbance is applied as a step signal to testify to the chattering elimination capabilities and robustness of the proposed control scheme. The DFIG speed response to the deterministic wind speed waveform is shown in Fig. 5. The zoomed-in view in Fig. 5(a) shows the chattering phenomenon in the speed waveform due to the discontinuous nature of the equivalent control law in SMC.On the other hand, both the STSMC and AISTSMC are of continuous nature, and successfully eliminates the

$$\begin{aligned}
1.\ T^{ref}_{em-AISTSMC} &= J\left(\dot{\omega}_{r-ref} - d_3 - \Theta_{\alpha\mathbf{E}}\,|\mathfrak{S}_E|^{\frac{1}{2}}\,\mathrm{sign}\,(\mathfrak{S}_\omega) - \Theta_{\beta\mathbf{E}}\int \mathrm{sign}\,(\mathfrak{S}_\omega)\right) \\
2.\ V^{ref}_{dr-AISTSMC} &= \sigma L_r\left(-G_1 + \frac{1}{\sigma L_r}R_r I_{dr} - \Theta_{\alpha\mathbf{E}}\,|\mathfrak{S}_E|^{\frac{1}{2}}\,\mathrm{sign}\,(\mathfrak{S}_1) - \Theta_{\beta\mathbf{E}}\int \mathrm{sign}\,(\mathfrak{S}_1)\right) \\
3.\ V^{ref}_{qr-AISTSMC} &= \sigma L_r\left(-G_2 + \frac{1}{\sigma L_r}R_r I_{qr} - \Theta_{\alpha\mathbf{E}}\,|\mathfrak{S}_E|^{\frac{1}{2}}\,\mathrm{sign}\,(\mathfrak{S}_2) - \Theta_{\beta\mathbf{E}}\int \mathrm{sign}\,(\mathfrak{S}_2)\right) \\
4.\ I^{ref}_{d-AISTSMC} &= \frac{1}{g_0(x)}\left(\dot{E}^* + \frac{1}{C}I_{0r} - \Theta_{\alpha\mathbf{E}}\,|\mathfrak{S}_E|^{\frac{1}{2}}\,\mathrm{sign}\,(\mathfrak{S}_E) - \Theta_{\beta\mathbf{E}}\int \mathrm{sign}\,(\mathfrak{S}_E)\right)
\end{aligned} \tag{81}$$

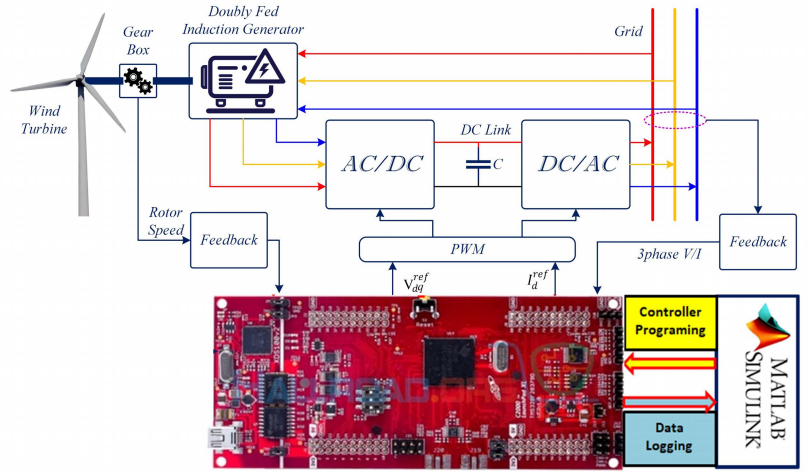

FIGURE 4. Experimental Setup.

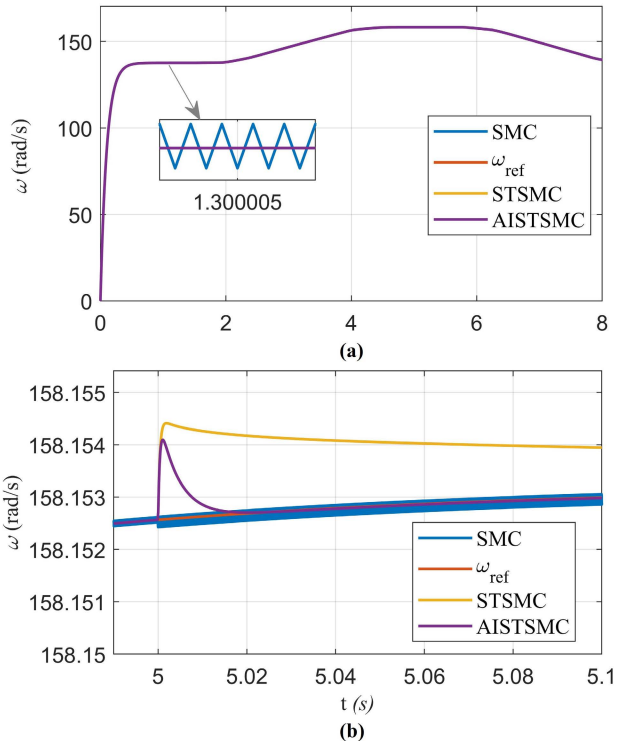

FIGURE 5. Reference speed tracking comparison under step disturbance conditions. (a) Normal view with chattering comparison. (b) Zoomed view depicting speed response at time of step uncertainty.

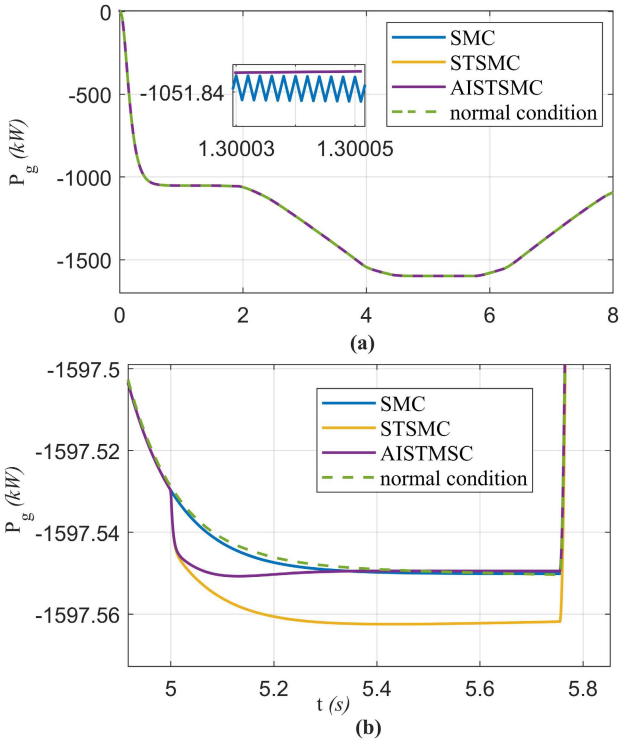

FIGURE 6. Active power comparison under step disturbance conditions. (a) Normal view with chattering comparison. (b) Zoomed view depicting active power at time of step uncertainty.

chattering in SMC. A step uncertainty is applied at $t = 5$ s and the response of the SMC, STSMC, and AISTSMC schemes is given in Fig. 5(b). The robust nature of SMC is evident from Fig. 5(b), as it shows a little deviation in response to the step uncertainty, but it loses its efficiency due to severe chattering. The lack of robustness described insection 3.3 is visible from the speed waveform in Fig. 5(b). It can be seen that the speed waveform for STSMC loses its tracking at $t = 5$ s and converges very slowly to the reference value. The ANN-based AISTSMC compensates for the STSMC problem and gives improved performance when step disturbance is applied. The speed deviation for STSMC is 158.1545 rad s^{-1} from reference value, whereas AISTSMC gives much lesser deviation of 158.154 rad s^{-1}. Similarly, the AISTSMC shows

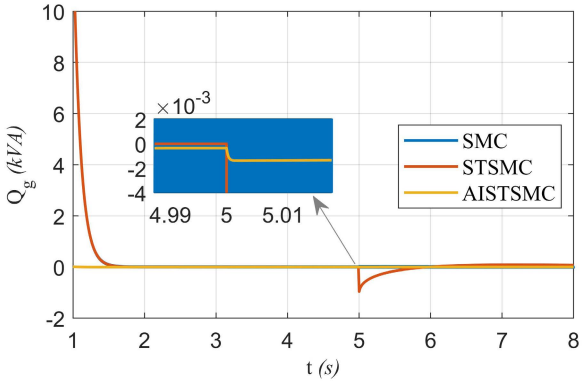

FIGURE 7. Reactive power comparison under step disturbance conditions.

faster convergence and converges back to the reference value after $t = 0.023$ s, whereas STSMC loses its convergence at this time.

The DFIG active power response to the deterministic wind speed waveform is compared in Fig. 6. The zoomed-in view in the Fig. 6(a) shows chattering in the active power waveform due to the discontinuous nature of the equivalent control law in SMC.Contrary, STSMC and AISTSMC gives smooth waveform with less chattering. The variation in active power for SMC, STSMC, and AISTSMC when step disturbance is applied is given in Fig. 6(b). The SMC shows robustness and has less deviation (compared to the active power under normal condition). Thelack of robustness in STSMC is visible from the active power waveform in Fig. 6(b). It can be seen that the active power waveform for STSMC deviates at a large scale compared to the active power under the normal condition at $t = 5$ s. The ANN-based AISTSMC compensates for the STSMC problem and gives improved performance when step disturbance is applied. The peak active power deviation for normal active power is 0.02 kW, whereas AISTSMC gives a much lesser deviation of 0.01 kW at $t = 5.1$ s. Similarly, the AISTSMC converges back to the normal power after $t = 0.398$ s, whereas STSMC loses convergence and provides excessive power of 0.01 kW at this point.

The DFIG reactive power response to the deterministic wind speed waveform is shown inFig. 7. The reactive power converges to zero in a finite-time. The zoomed-in view in Fig. 7 shows excessive chattering in reactive power under the SMC scheme due to the discontinuous nature of the equivalent control law. A step uncertainty is applied at $t = 5$ s and the response of the SMC, STSMC, and AISTSMC schemes is given in Fig. 7. The robustness of SMC is evident from the figure, as it shows a little deviation from zero, but it loses its efficiency due to severe chattering. The STSMC disadvantages of less robustness is evident from the reactive power waveform in Fig. 7. It can be seen that the reactive power waveform for STSMC deviates from 0 K VAR at $t = 5$ s and converges very slowly to the zero value. The ANN-based AISTSMC compensates for the STSMC problems and gives improved performance when step disturbance is applied.

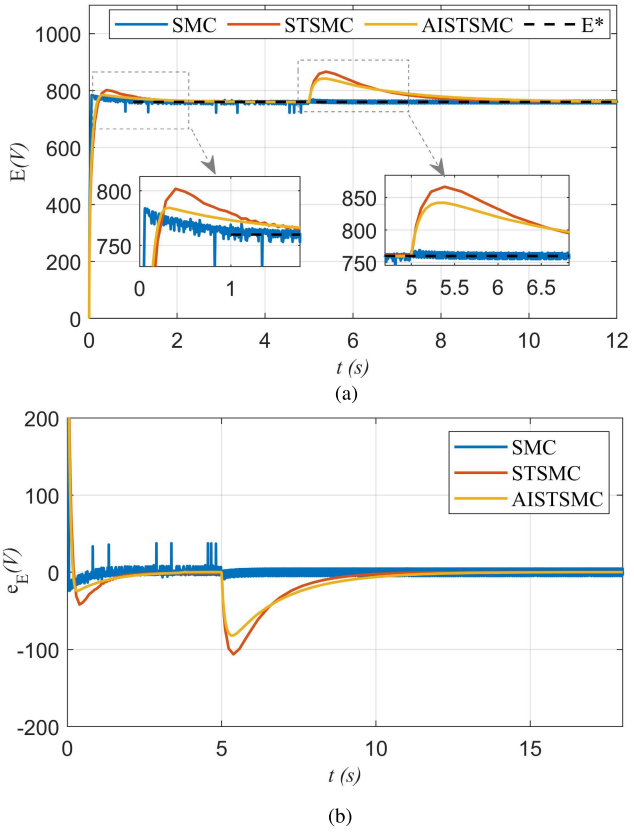

FIGURE 8. Grid side performance analysis. (a) DC Link Voltage comparison under step disturbance. (b) DC-link voltage error comparison under step disturbance.

The reactive power deviation for STSMC is 0.807 k VAR from zero value, whereas AISTSMC gives much lesser deviation of 0.0013 kVAR. Similarly the AISTSMC converges back to the zero value after $t = 0.05$ s, whereas STSMC convergence to zero after $t = 1$ s.

A similar analysis is also made for grid-side control. The DC link response to the deterministic wind speed waveform is shown in Fig. 8. A constant voltage of 760 V is selected as reference voltage (E^*). It can be observed that SMC is showinga fast convergence of 0.97 s, but it suffers from severe chattering in the V_{DC}. The SMC shows an overshoot 18.1 V, STSMC offers a larger overshoot of 40 V, whereas the AISTSMC has a lesser overshoot of 23 V with improved and much smoother V_{DC}. Similarly, at $t = 5$ s, where a step uncertainty is applied, the SMC offers good robustness followed by AISTSMC with an overshoot of 8 V. The STSMC, due to less robustness, offers a high overshoot of 106 V compared to the proposed AISTSMC scheme that offers an overshoot of 80 V. Thus, it is validated that the STSMC exhibits inherent chattering elimination feature due to its continuous nature, whereas the AISTSMC enjoys both the robustness and chattering elimination features and proves itself to be a viable option for DFIG-based WECS. The error waveform for the V_{DC} is shown in Fig. 8 (b) where it is clear that the AISTSMC provides less error than the STSMC scheme.

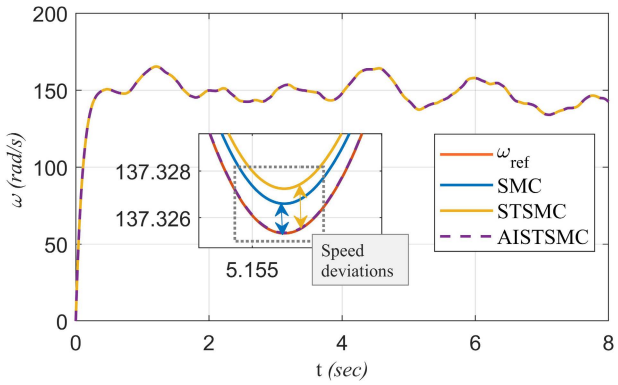

FIGURE 9. Rotor speed convergence comparison under lumped disturbance.

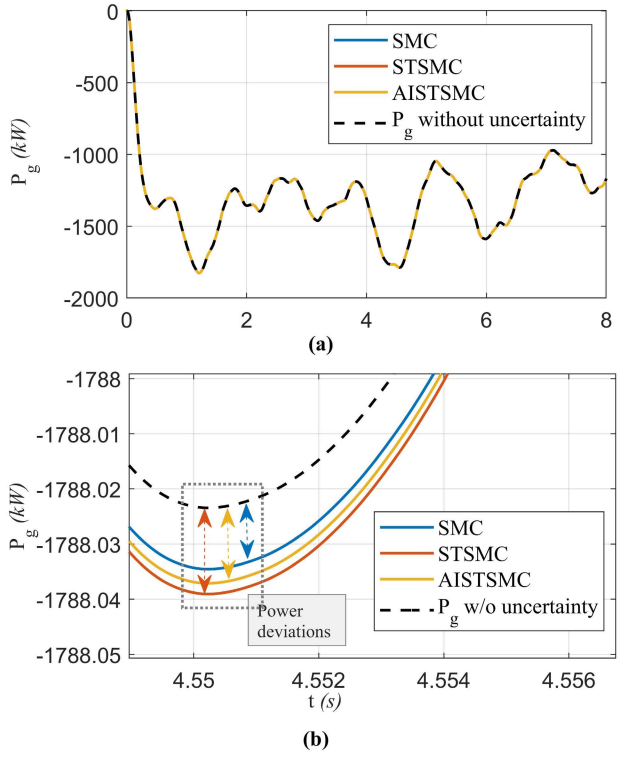

FIGURE 10. Active power comparison under lumped disturbance. (a) Normal view. (b) Zoomed view depicting variation in active power under lumped disturbance.

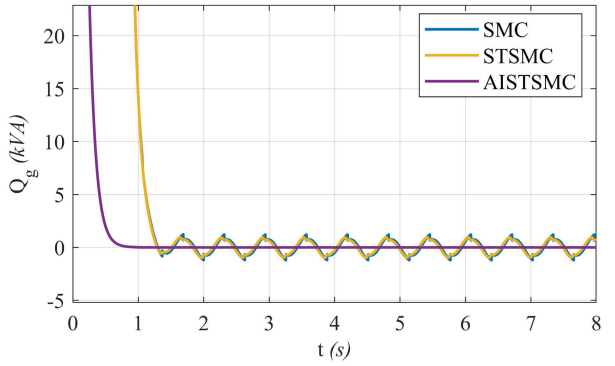

FIGURE 11. Reactive power comparison under lumped disturbance.

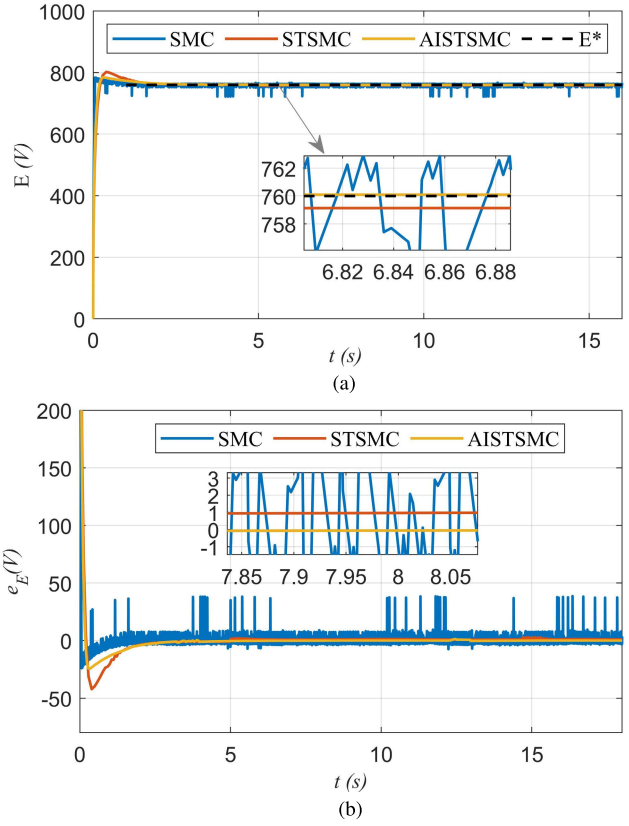

FIGURE 12. Grid side performance analysis under lumped disturbance. (a) DC Link Voltage comparison. (b) DC-link voltage error comparison.

B. CASE 2: PERFORMANCE EVALUATION UNDER PARAMETRIC UNCERTAINTIES AND DISTURBANCES

In this test, a lumped uncertainty $d(t)$ commissioning external and parametric uncertainty with 25% variation is added to the DFIG-based WECS. This uncertainty is mathematically expressed as follows:

$$\left.\begin{aligned} \dot{x} &= F(x) + Hu = f(x) + hu + d(t) \\ d(t) &= 25\%f(x) + 25\%hu + 2 - \sin(\omega t) \end{aligned}\right\} \quad (82)$$

A similar disturbance imitating 25 % variation is also added to the grid side and expressed as follows:

$$dE = 25\%g(x) + 5\sin(\omega t) \quad (83)$$

The DFIG speed response to the stochastic wind waveform is shown in Fig. 9. The zoomed-in view in Fig. 9 shows that the SMC has robust performance as compared to the STSMC scheme under lumped uncertainties. The total deviation for SMC is $0.02\,\mathrm{rad\,s^{-1}}$, whereas the deviation for STSMC is $0.03\,\mathrm{rad\,s^{-1}}$, which is much higher than the SMC scheme. On the other hand, the AISTSMC shows a negligible deviation under lumped uncertainties. It can be seen from Fig. 10 that the active power waveform for STSMC deviates at a large scale as compared to the active power under the normal condition at $t = 5\,\mathrm{s}$. The ANN-based AISTSMC compensates for the STSMC problem and gives improved performance when step disturbance is applied. The active

TABLE 3. Parameters [36].

DFIG and Wind Turbine Parameter	Values	Control Parameters	Values
λ_{opt}	6.325	k	$0.5-5$
No. of pole pairs	3	γ	0.7
Rs	1.4Ohm	α	0.8
Rr	1.2Ohm	k_1	0.02
M	0.0051839H	k_2	5
$Lr = L_S$	0.0053H	k_3	0.005
f_f	0.00015Nms^{-1}	k_4	1
J	765.6kg/m^2	α_1	0.0015
DC Link Voltage (E)	760V	α_2	5
DC Link Capacitor	0.01 farad	α_E	0.02
Frequency	50Hz	α_ω	5
Blade radius	35m		
Gear ratio	62.5		

power deviation as compared to power under normal conditions, shown in Fig. 10 (b), is 0.01 kW for SMC, 0.018 kWfor STSMC, and 0.013 kWfor AISTSMC.

The DFIG reactive power response to the stochastic wind speed waveform under lumped uncertainty is shown in Fig. 11. The reactive power converges to zero in a finite-time. Fig. 11 shows excessive oscillations in the reactive power using the SMC scheme and STSMC scheme due to the lumped uncertainty. On the other hand, the AISTSMC scheme exhibits significant robustness to the lumped uncertainties. It can be seen that the reactive power waveform for SMC and STSMC schemes have a similar response, whereas the ANN-based AISTSMC scheme compensates for the STSMC problems and gives improved performance under lumped uncertainties. The AISTSMC converges to the zero value at $t = 0.7$ s, whereas SMC and STSMC are much slower with a convergence time of 1.2 s.

A similar analysis is also carried out for the grid-side control. The DC link response to the stochastic wind speed waveform is shown in Fig. 12 (a). A constant voltage of 760 V is selected as a reference voltage (E^*). It can be seen that SMC is showing a fast convergence of 0.36 s with an overshoot of 22 V, but it suffers from severe chattering in the V_{DC}. The STSMC offers a larger overshoot of 42.2 V, whereas the AISTSMC has a lesser overshoot of 24 V with improved and much smoother V_{DC}. Similarly, in case of lumped uncertainty, the SMC performance is deteriorated in terms of chattering and unwanted oscillations.The STSMC shows the highest steady state error of 1 V as compared to reference value, whereas the AISTSMC shows an almost negligible steady state error . The error plot in Fig. 12 (b) also verifies the robustness and chattering elimination of the proposed AISTSMC scheme. It can be seen that STSMC provides an error of 1 V, whereas the AISTSMC gives an almost negligible error.

VI. CONCLUSION

For DFIG-based WECS, this research presents a high-performance super-twisting sliding mode control (STSMC) synergized with the artificial neural network. The suggested control scheme is a hybrid of artificial intelligence and STSMC that addresses the problem of robustness of STSMC schemes while retaining system robustness and stability. To eliminate the lack of robustness in STSMC, the signum function is initially replaced by a super-twisting algorithm. Then, to improve the robustness of the STSMC-based system, the ANN theory is introduced which increases the robustness against external disturbances and parametric uncertainties. Under uncertain situations, the performance of the ANN-based STSMC approach is compared with the SMC and STSMC benchmarks. The suggested technique outperforms the SMC and STSMC in terms of lowest chattering, quick dynamic response, higher accuracy, and disturbance rejection. It is evident from the DC link voltage that the SMC offers an overshoot of 8 V, STSMC offers a high overshoot of 106 V, and the proposed AISTSMC scheme offers 80 V. In summary, the results show that the ANN-based control method established in this study is a viable and desired option for DFIG-based WECS.

REFERENCES

[1] (2018). *Word Energy Balances*. [Online]. Available: https://webstore.iea.org/download/direct/2263filenamewörld_energy_balances_2018_overview.pdf

[2] I. Sami, S. Ullah, N. Ullah, and J.-S. Ro, "Sensorless fractional order composite sliding mode control design for wind generation system," *ISA Trans.*, vol. 111, pp. 275–289, May 2020.

[3] M. S. Nazir, N. Ali, M. Bilal, and H. M. Iqbal, "Potential environmental impacts of wind energy development: A global perspective," *Current Opinion Environ. Sci. Health*, vol. 13, pp. 85–90, Feb. 2020.

[4] R. C. Sonderegger, D. Henderson, S. Bubb, and J. Steury, "Distributed asset insight," *IEEE Power Energy Mag.*, vol. 2, no. 3, pp. 32–39, May 2004.

[5] H. B. Puttgen, P. R. MacGregor, and F. C. Lambert, "Distributed generation: Semantic hype or the dawn of a new era?" *IEEE Power Energy Mag.*, vol. 1, no. 1, pp. 22–29, Jan. 2003.

[6] S. Rahman, "Green power: What is it and where can we find it?" *IEEE Power Energy Mag.*, vol. 1, no. 1, pp. 30–37, Jan./Feb. 2003.

[7] G. J. I. P. Martin and E. Magazine, "Renewable energy gets the 'green' light Chicago," *IEEE Power Energy Mag.*, vol. 1, no. 6, pp. 34–39, Nov. 2003.

[8] B. Beltran, T. Ahmed-Ali, and M. E. H. Benbouzid, "Sliding mode power control of variable-speed wind energy conversion systems," *IEEE Trans. Energy Convers.*, vol. 23, no. 2, pp. 551–558, Jun. 2008.

[9] S. M. Mozayan, M. Saad, H. Vahedi, H. Fortin-Blanchette, and M. Soltani, "Sliding mode control of PMSG wind turbine based on enhanced exponential reaching law," *IEEE Trans. Ind. Electron.*, vol. 63, no. 10, pp. 6148–6159, Oct. 2016.

[10] B. Kelkoul and A. J. E. Boumediene, "Stability analysis and study between classical sliding mode control (SMC) and super twisting algorithm (STA) for doubly fed induction generator (DFIG) under wind turbine," *Energy*, vol. 118871, Jan. 2020, Art. no. 118871.

[11] V. Utkin and H. Lee, "Chattering problem in sliding mode control systems," in *Proc. Int. Workshop Variable Struct. Syst. (VSS)*, Jun. 2006, pp. 346–350.
[12] S. M. Mozayan, M. Saad, H. Vahedi, H. Fortin-Blanchette, and M. Soltani, "Sliding mode control of PMSG wind turbine based on enhanced exponential reaching law," *IEEE Trans. Ind. Electron.*, vol. 63, no. 10, pp. 6148–6159, Oct. 2016.
[13] D. Milosavljevic, "General conditions for existence of a quasi-sliding mode on the switching hyperplane in discrete variable structure systems," *Autom. Remote Control*, vol. 46, pp. 307–314, Jan. 1985.
[14] A. Bartoszewicz, "Discrete-time quasi-sliding-mode control strategies," *IEEE Trans. Ind. Electron.*, vol. 45, no. 4, pp. 633–637, Apr. 1998.
[15] R. B. N. Ngadungon and Y. B. M. Sam, "Discrete time sliding mode control using multirate output feedback to reduce chattering," in *Proc. IEEE Student Conf. Res. Develop. (SCOReD)*, Dec. 2010, pp. 236–239.
[16] J. Y. Hung, W. Gao, and J. C. Hung, "Variable structure control: A survey," *IEEE Trans. Ind. Electron.*, vol. 40, no. 1, pp. 2–22, Feb. 1993.
[17] I. Sami, S. Ullah, A. Basit, N. Ullah, and J.-S. J. Ro, "Integral super twisting sliding mode based sensorless predictive torque control of induction motor," *IEEE Access*, vol. 8, pp. 186740–186755, 2020.
[18] J. Wang, D. Bo, Q. Miao, Z. Li, X. Wu, and D. J. Lv, "Maximum power point tracking control for a doubly fed induction generator wind energy conversion system based on multivariable adaptive super-twisting approach," *Int. J. Electr. Power Energy Syst.*, vol. 124, Jan. 2021, Art. no. 106347.
[19] B. Beltran, T. Ahmed-Ali, and M. Benbouzid, "High-order sliding-mode control of variable-speed wind turbines," *IEEE Trans. Ind. Electron.*, vol. 56, no. 9, pp. 3314–3321, Sep. 2009.
[20] I. Sami, S. Ullah, Z. Ali, N. Ullah, and J.-S. Ro, "A super twisting fractional order terminal sliding mode control for DFIG-based wind energy conversion system," *Energies*, vol. 13, no. 9, p. 2158, 2020.
[21] A. Benamor, M. Benchouia, K. Srairi, and M. Benbouzid, "A novel rooted tree optimization apply in the high order sliding mode control using super-twisting algorithm based on DTC scheme for DFIG," *Int. J. Electr. Power Energy Syst.*, vol. 108, pp. 293–302, Jun. 2019.
[22] A. Dávila, J. A. Moreno, and L. Fridman, "Variable gains super-twisting algorithm: A Lyapunov based design," in *Proc. Amer. Control Conf.*, Jun. 2010, pp. 968–973.
[23] V. Utkin, J. Guldner, and J. Shi, *Sliding Mode Control in Electromechanical Systems*. Boca Raton, FL, USA: CRC Press, 2017.
[24] V. I. Utkin, *Sliding Modes in Control and Optimization*. Cham, Switzerland: Springer, 2013.
[25] T. Gonzalez, J. A. Moreno, and L. Fridman, "Variable gain super-twisting sliding mode control," *IEEE Trans. Autom. Control*, vol. 57, no. 8, pp. 2100–2105, Aug. 2013.
[26] C. Evangelista, P. Puleston, F. Valenciaga, and L. M. Fridman, "Lyapunov-designed super-twisting sliding mode control for wind energy conversion optimization," *IEEE Trans. Ind. Electron.*, vol. 60, no. 2, pp. 538–545, Feb. 2013.
[27] C. Evangelista, P. Puleston, F. Valenciaga, and A. Dávila, "Variable gains super-twisting control for wind energy conversion optimization," in *Proc. 11th Int. Workshop Variable Struct. Syst. (VSS)*, Jun. 2010, pp. 50–55.
[28] B. Soufyane, R. Abdelhamid, and Z. Smail, "Fuzzy-variable gain super twisting algorithm control design for direct-drive PMSG wind turbines," in *Proc. IEEE 58th Conf. Decis. Control (CDC)*, Dec. 2019, pp. 4885–4890.
[29] H. Benbouhenni, Z. Boudjema, and A. Belaidi, "DPC based on ANFIS super-twisting sliding mode algorithm of a doubly-fed induction generator for wind energy system," *J. Européen des Systèmes Automatisés*, vol. 53, no. 1, pp. 69–80, 2020.
[30] H. Obeid, S. Laghrouche, and L. Fridman, "A barrier function based-adaptive super-twisting controller for wind energy conversion system," in *Proc. IEEE 58th Conf. Decis. Control (CDC)*, Dec. 2019, pp. 7869–7874.
[31] V. T. Nguyen, C. Y. Lin, S. F. Su, and Q. V. Tran, "Adaptive chattering free neural network based sliding mode control for trajectory tracking of redundant parallel manipulators," *Asian J. Control*, vol. 21, no. 2, pp. 908–923, 2019.
[32] F. F. El-Sousy and F. A. Alenizi, "Optimal adaptive super-twisting sliding-mode control using online actor-critic neural networks for permanent-magnet synchronous motor drives," *IEEE Access*, vol. 9, pp. 82508–82534, 2021.
[33] F. F. El-Sousy, M. M. Amin, G. A. A. Aziz, and O. A. Mohammed, "Robust adaptive neural-network super-twisting sliding-mode control for PMSM-driven linear stage with uncertain nonlinear dynamics," in *Proc. IEEE Transp. Electrific. Conf. Expo. (ITEC)*, Jun. 2020, pp. 87–92.
[34] F. Valenciaga and P. F. Puleston, "High-order sliding control for a wind energy conversion system based on a permanent magnet synchronous generator," *IEEE Trans. Energy Convers.*, vol. 23, no. 3, pp. 860–867, Sep. 2008.
[35] B. Beltran, M. E. H. Benbouzid, and T. Ahmed-Ali, "Second-order sliding mode control of a doubly fed induction generator driven wind turbine," *IEEE Trans. Energy Convers.*, vol. 27, no. 2, pp. 261–269, Jun. 2012.
[36] C. Evangelista, P. Puleston, F. Valenciaga, and L. M. Fridman, "Lyapunov-designed super-twisting sliding mode control for wind energy conversion optimization," *IEEE Trans. Ind. Electron.*, vol. 60, no. 2, pp. 538–545, Feb. 2013.
[37] C. Evangelista, F. Valenciaga, and P. Puleston, "Active and reactive power control for wind turbine based on a MIMO 2-sliding mode algorithm with variable gains," *IEEE Trans. Energy Convers.*, vol. 28, no. 3, pp. 682–689, Sep. 2013.
[38] M. Benbouzid, B. Beltran, Y. Amirat, G. Yao, J. Han, and H. Mangel, "Second-order sliding mode control for DFIG-based wind turbines fault ride-through capability enhancement," *ISA Trans.*, vol. 53, no. 3, pp. 827–833, May 2014.
[39] A. Merabet, K. T. Ahmed, H. Ibrahim, and R. Beguenane, "Implementation of sliding mode control system for generator and grid sides control of wind energy conversion system," *IEEE Trans. Sustain. Energy*, vol. 7, no. 3, pp. 1327–1335, Jul. 2016.
[40] M. J. Morshed and A. Fekih, "A new fault ride-through control for DFIG-based wind energy systems," *Electr. Power Syst. Res.*, vol. 146, pp. 258–269, May 2017.
[41] C. A. Evangelista, A. Pisano, P. Puleston, and E. Usai, "Receding horizon adaptive second-order sliding mode control for doubly-fed induction generator based wind turbine," *IEEE Trans. Control Syst. Technol.*, vol. 25, no. 1, pp. 73–84, Jan. 2017.
[42] Y. Berrada and I. Boumhidi, "New structure of sliding mode control for variable speed wind turbine," *IFAC J. Syst. Control*, vol. 14, Dec. 2020, Art. no. 100113.
[43] M. J. Karabacak, "A new perturb and observe based higher order sliding mode MPPT control of wind turbines eliminating the rotor inertial effect," *Renew. Energy*, vol. 133, pp. 807–827, Apr. 2019.
[44] E. H. Dursun and A. A. J. Kulaksiz, "Second-order sliding mode voltage-regulator for improving MPPT efficiency of PMSG-based WECS," *Int. J. Electr. Power Energy Syst.*, vol. 121, Oct. 2020, Art. no. 106149.
[45] L. Xiong, P. Li, and J. J. Wang, "High-order sliding mode control of DFIG under unbalanced grid voltage conditions," *Int. J. Electr. Power Energy Syst.*, vol. 117, May 2020, Art. no. 105608.
[46] B. Kelkoul and A. J. Boumediene, "Stability analysis and study between classical sliding mode control (SMC) and super twisting algorithm (STA) for doubly fed induction generator (DFIG) under wind turbine," *Energy Convers. Manage.*, vol. 214, Jan. 2020, Art. no. 118871.
[47] J. Wang, D. Bo, Q. Miao, Z. Li, X. Wu, and D. Lv, "Maximum power point tracking control for a doubly fed induction generator wind energy conversion system based on multivariable adaptive super-twisting approach," *Int. J. Electr. Power Energy Syst.*, vol. 124, Jan. 2021, Art. no. 106347.
[48] L. Fridman, J. A. Moreno, B. Bandyopadhyay, S. Kamal, and A. Chalanga, "Continuous nested algorithms: The fifth generation of sliding mode controllers," in *Recent Advances in Sliding Modes: From Control to Intelligent Mechatronics*. Cham, Switzerland: Springer, 2015, pp. 5–35.
[49] B. Beltran, M. E. H. Benbouzid, and T. Ahmed-Ali, "Second-order sliding mode control of a doubly fed induction generator driven wind turbine," *IEEE Trans. Energy Convers.*, vol. 27, no. 2, pp. 261–269, Jun. 2012.
[50] Y. Bekakra and D. B. Attous, "Sliding mode controls of active and reactive power of a DFIG with MPPT for variable speed wind energy conversion," *Austral. J. Basic Appl. Sci.*, vol. 5, no. 12, pp. 2274–2286, 2011.
[51] S. Ebrahimkhani, "Robust fractional order sliding mode control of doubly-fed induction generator (DFIG)-based wind turbines," *ISA Trans.*, vol. 63, pp. 343–354, Jul. 2016.
[52] M. Machmoum and F. Poitiers, "Sliding mode control of a variable speed wind energy conversion system with DFIG," in *Proc. Int. Conf. Exhib. Ecolog. Vehicles Renew. Energies, (MONACO)*, Mar. 2009, pp. 26–29.
[53] X. Liu, Y. Han, and C. J. Wang, "Second-order sliding mode control for power optimisation of DFIG-based variable speed wind turbine," *IET Renew. Power Gener.*, vol. 11, no. 2, pp. 408–418, 2016.
[54] L. Xiong, P. Li, F. Wu, M. Ma, M. W. Khan, and J. J. Wang, "A coordinated high-order sliding mode control of DFIG wind turbine for power optimization and grid synchronization," *Int. J. Electr. Power Energy Syst.*, vol. 105, pp. 679–689, Feb. 2019.

[55] B. Beltran, M. Benbouzid, and T. Ahmed-Ali, "High-order sliding mode control of a DFIG-based wind turbine for power maximization and grid fault tolerance," in *Proc. IEEE Int. Electr. Mach. Drives Conf.*, May 2009, pp. 183–189.
[56] A. Levant, "Higher-order sliding modes, differentiation and output-feedback control," *Int. J. Control*, vol. 76, nos. 9–10, pp. 924–941, Jan. 2003.
[57] S. Benelghali, M. E. H. Benbouzid, J. F. Charpentier, T. Ahmed-Ali, and I. Munteanu, "Experimental validation of a marine current turbine simulator: Application to a permanent magnet synchronous generator-based system second-order sliding mode control," *IEEE Trans. Ind. Electron.*, vol. 58, no. 1, pp. 118–126, Jan. 2011.
[58] S. E. B. Elghali, M. E. H. Benbouzid, T. Ahmed-Ali, and J. F. Charpentier, "High-order sliding mode control of a marine current turbine driven doubly-fed induction generator," *IEEE J. Ocean. Eng.*, vol. 35, no. 2, pp. 402–411, Apr. 2010.
[59] C. Zhang, S. Gutierrez, F. Plestan, and J. J. I.-P. de León-Morales, "Adaptive super-twisting control of floating wind turbines with collective blade pitch control," *IFAC-PapersOnLine*, vol. 52, no. 4, pp. 117–122, 2019.
[60] H. Chen, Q. Li, S. Tang, N. AÏT-Ahmed, J. Han, T. Wang, Z. Zhou, T. Tang, and M. Benbouzid, "Adaptive super-twisting control of doubly salient permanent magnet generator for tidal stream turbine," *Int. J. Electr. Power Energy Syst.*, vol. 128, Jun. 2021, Art. no. 106772.
[61] Y. Shtessel, M. Taleb, and F. Plestan, "A novel adaptive-gain supertwisting sliding mode controller: Methodology and application," *Automatica*, vol. 48, no. 5, pp. 759–769, 2012.

IRFAN SAMI (Graduate Student Member, IEEE) received the B.Sc. degree in electrical engineering from the University of Engineering and Technology Peshawar, Bannu Campus, Pakistan, in 2016, and the M.Sc. degree in electrical engineering from COMSATS University Islamabad, Abbottabad Campus, Abbottabad, Pakistan, in 2019. He is currently pursuing the Ph.D. degree in electrical engineering with Chung-Ang University, Seoul, South Korea. His research interests include electric drives, renewable energies, and electrical machine design.

SHAFAAT ULLAH was born in Lakki Marwat, Pakistan. He received the B.Sc. and M.Sc. degrees in electrical engineering from the University of Engineering and Technology Peshawar, Pakistan, in 2007 and 2013, respectively. He is currently pursuing the Ph.D. degree in electrical engineering with COMSATS University Islamabad, Abbottabad Campus, Abbottabad, Pakistan.

He served as an Assistant Director for the Pakistan Council of Renewable Energy Technologies (PCRET), and as an Assistant Manager (Operation)/Junior Engineer (Electrical) for Lahore Electric Supply Company (LESCO), Pakistan. He is currently serving as an Assistant Professor with the Department of Electrical Engineering, University of Engineering and Technology Peshawar, Bannu Campus, Pakistan. His research interests include photovoltaics, wind energy conversion systems, and distributed control of multiagent systems-based microgrids/smart grids.

SAREER UL AMIN was born in Swabi, Pakistan. He received the B.S. degree in computer science from the Islamia College University Peshawar, Pakistan, in 2016 and 2020, respectively. He is currently pursuing the M.S. degree in computer science and engineering with Chung-Ang University, Seoul, South Korea. He was a Research Assistant with the Digital Image Processing Laboratory (DIP), Islamia College University Peshawar. His research interests include computer vision, deep learning, and machine learning.

AHMED AL-DURRA (Senior Member, IEEE) received the Ph.D. degree in ECE from The Ohio State University in 2010. He is currently a Professor with the EECS Department, Khalifa University, United Arab Emirates. He has one U.S. patent, one edited book, 12 book chapters, and over 230 scientific articles in top-tier journals and refereed international conference proceedings. He has supervised/co-supervised over 30 Ph.D./master's students. He is leading the Energy Systems Control and Optimization Laboratory under the Advanced Power and Energy Center. His research interests include applications of control and estimation theory on power systems stability, micro and smart grids, renewable energy systems and integration, and process control. He is an Editor of IEEE TRANSACTIONS ON SUSTAINABLE ENERGY and IEEE POWER ENGINEERING LETTERS and an Associate Editor of IEEE TRANSACTIONS ON INDUSTRY APPLICATIONS, *IET Renewable Power Generation*, and *Frontiers in Energy Research*.

NASIM ULLAH received the Ph.D. degree in mechatronics engineering from Beihang University, Beijing, China, in 2013. From 2006 to 2010, he was a Senior Design Engineer with IICS, Pakistan. He is currently an Associate Professor of electrical engineering with Taif University, Saudi Arabia. His research interests include renewable energy, flight control systems, integer and fractional order modeling of dynamic systems, integer/fractional order adaptive robust control methods, fuzzy/NN, hydraulic and electrical servos, epidemic, and vaccination control strategies.

JONG-SUK RO received the B.S. degree in mechanical engineering from Han-Yang University, Seoul, South Korea, in 2001, and the Ph.D. degree in electrical engineering from Seoul National University (SNU), Seoul, in 2008.

He is currently an Associate Professor with the School of Electrical and Electronics Engineering, Chung-Ang University, Seoul. In 2014, he was with the University of Bath, Bath, U.K., as an Academic Visitor. From 2013 to 2016, he worked with the Brain Korea 21 Plus, SNU, as a BK Assistant Professor. He conducted research at the Electrical Energy Conversion Systems Research Division, Korea Electrical Engineering and Science Research Institute, as a Researcher, in 2013. From 2012 to 2013, he was with the Brain Korea 21 Information Technology of SNU, as a Postdoctoral Fellow. He conducted research at the Research and Development Center of Samsung Electronics as a Senior Engineer, from 2008 to 2012. His research interests include the analysis and optimal design of next-generation electrical machines using smart materials, such as electromagnets, piezoelectric, and magnetic shape memory alloys.